Looking for Permeability: Mass and Heat Flow Assessment Using High Resolution soil CO_2 Flux Surveys within the Taupo Volcanic Zone, New Zealand

A thesis submitted in partial fulfilment of the requirements for the degree of

Master of Science in Geology

at the

Department of Geological Sciences

University of Canterbury

By

Simon H. Bloomberg

University of Canterbury

2012

Frontispiece

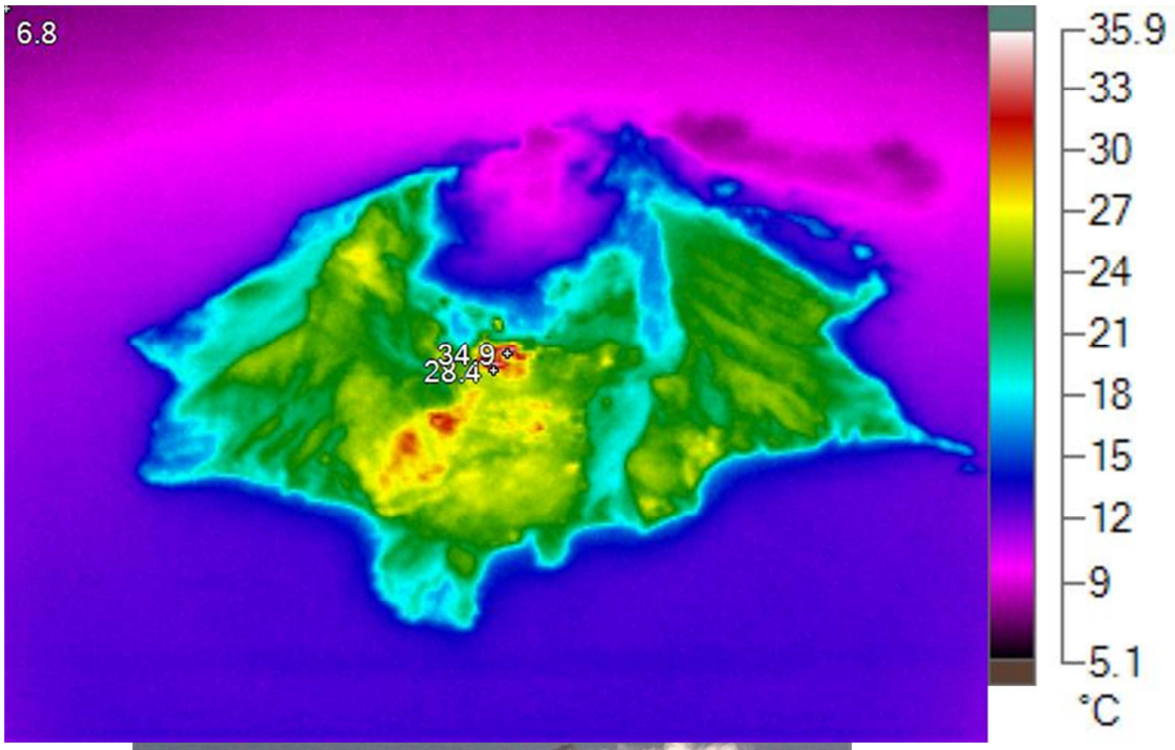

Thermal infra-red and true colour images of White Island taken during November 2011.

Abstract

Soil CO2 flux (φCO_2) has increasingly become important as a global exploration and monitoring tool in geothermal and volcanic fields. As CO_2 is the second most abundant gas in magma-hydrothermal systems, its study is vital for the location or management of those systems. Often one of the only surface expressions is the diffuse gas flux streaming through the soil zone. This thesis reports the investigations into heat and mass at the Rotokawa geothermal field's thermal area, and White Island volcano's crater floor hydrothermal system. Surface measurements were taken at high spatial resolution across the fields in a large sampling campaign during the summers of 2010/2011 and 2011/2012. A large dataset was built up which allowed for greater accuracy during geospatial modelling. The models are 2d pixel plots of the soil gas flux and temperature and are used to estimate values of heat and mass flow for the respective magma-hydrothermal systems.

Both field areas have a large anomalous diffuse gas flux through the soil zone and related conductive heat flow anomaly, which indicates relative permeability from the source to the surface in these areas. That the rising fluids from the deep source can be sampled at the surface simply is a powerful tool for the exploration and management of these systems. Rotokawa has a diffuse gas release of over 600 t d^{-1} and an associated heat flow through soil of 37 MW_t while White Island has a diffuse gas release of 116 t d^{-1} and 19.5 MW_t of heat flow through the soil. Translating these values to total heat and mass flow values: Rotokawa has a mass flow 125 kg s^{-1} and a heat flow of 314 MW_t and White Island's crater floor has a mass flow of 100 kg s^{-1} and a heat flow of 22 MW_t.

Fluid flow pathways are mapped from the surface and show arcuate and hot spot spatiality, controlled by fault related permeability and structure. soil gas and temperature surveying elucidates Shallow structures that otherwise may have been hidden from status quo surface mapping. The method used in this study is applicable to both known thermal areas and blind thermal areas by addressing not only the flux but also the nature of the soil gases.

Further study of White Island has found more evidence for the existence of seawater infiltration of the crater magma-hydrothermal system.

Acknowledgements

First and foremost I give thanks to my supervisory team: To Dr. Clinton Rissmann, who counselled and trained me in the way of the flux, who even with a young family encouraged me to share his home and bestowed upon me an enthusiasm for collecting data I didn't think I would ever have. Cheers mate! To Dr. Agnes Mazot, merci de votre patience et pour m'aider avec la vie de GNS Wairakei, I hope you stay in NZ and flux all of the TVZ! To Dr. Travis Horton, you're a top warlock and a top supervisor; you're effort in running the gas samples turned my thesis from good to great! To Dr. Christoper Oze, a late comer but a quick learner, and the man with the whip who really got me there, I owe you quite a lot of beer I feel. Meet you at Antonio's in five? Special thanks to Dr. Cindy Werner for her expert reviews, too little to late is better than none! To Dr. Darren Gravley, word. Thanks for getting me on board all those years ago (2? 3?), you turned an alright university experience into a really great one. I seriously am grateful for all the opportunities you've given me. Hopefully I can return the favour at some stage! And finally to Dr. Ben Kennedy, cheers. You got me into to this at Oamaru when I received my drawing of a volcano back with the grade "5/5 Wicked". I was stoked, I had always struggled with geology as a passion, but from then on I was hooked!

I have learnt so much over the last 3 years: how to be invited to a meeting, how to participate in a meeting, how to not turn up to a meeting, how to meet people in a meeting, how to organise my own meetings, how to organise other people to have meetings. I really learnt the value of meetings. I also really learnt the value of friendship, so I have to shout out to my flatmates, who really were mates and not just people I lived with, you know who you are, heaps of love! Shout out to the Warlocks, for keeping me in the scene even though I'm an old fart. Shout out to Courtney, it was up and down, and on and off… but you were a great friend and I learnt a lot, so for that I'm grateful. Shout out to Gladwin and Josh for getting me surfing, some of the most fun I've ever had, I'll see you at the beach sometime boys! Shout out to my fellow postgraduates, keep it up! Finally, a shoutout to my undergrad class of 2006, you made geology bearable and then alright and then not too bad and now look at me, the last one at UC, well now I've finished! I bet captain Jarg would be proud.

Thanks must also be given to all those others who helped me along the way, to those from the University of Canterbury: Dr. Anekant, Dr. Cole, Dr. Quigley, Dr. Bassett, Dr. Reid, Dr. Wilson, Dr. Turbull, Dr. Hampton, Dr. Nobes, Dr. Ring, Dr. Weaver, Dr. Grimshaw, Dr.Shulmeister and even DHB! You all gave me the time of day at one stage and that is all it takes! To those from GNS Science: Jeremy Cole-Baker, Karen Britten, Cindy Werner, Bruce Christenson, Gill Jolly, Brad Scott, Shelley, and Sue! To all those at Mighty River Power Ltd.: Jeremy O'Brien, Simon Addison, Jeff Winick, Tom Powell, Linda Price and Joe Gamman.

To the those who helped with fieldwork: Joanna Pawson, Mark Letham, Jelte Keeman, Heather Bickerton, Johanna Bloomberg, Karen Britten, Agnes Mazot, Clinton Rissmann; big up! You are the bread and butter and gave graciously of your time and energy. A Special big up goes to Jo and Joh, because you're both so rad, in and out of the field. I had such a good time in Taupo!

Finally I have to give the biggest shoutout to my whanau: the Elliots, the Bloombergs, The Barnfields and the Lawrences, you guys have supported me from day one to day 8945. I love you all so much and dedicate this thesis to you guys. Arohanui, much love!

Chur,

Si.

Table of Contents

Title Page i

Frontispiece ii

Abstract iii

Acknowledgements iv

List of Tables ix

List of Figures ix

Prologue 1

Chapter 1 2

SOIL CO2 EMISSIONS AS A PROXY FOR ASSESSMENT OF HEAT AND MASS FLOW, TAUPO VOLCANIC ZONE, NEW ZEALAND 2

1. Abstract 3

2. Introduction 4

3. Geological Setting 5

3.1 Rotokawa (RK) 5

3.2 White Island (WI) 6

4. Methods & Materials 6

4.1 Soil gas flux and temperature measurements 6

4.2 Carbon isotopic analysis of soil gas 8

4.3 Data Analysis 8

4.4 Heat and mass flow from soil temperature 9

4.5 Heat and mass flow and emissions calculations from CO_2 flux 11

5. Results 12

5.1 Rotokawa: Diffuse soil gas fluxes, stable isotopes and soil temperatures 12

5.2 Rotokawa: φH2S and relationships with φCO2 13

5.3 White Island: Diffuse soil gas fluxes, stable isotopes and soil temperatures 13

5.4 Heat and mass flow based on soil temperature measurements 14

5.5 Heat and mass flow calculated from CO_2 degassing 14

6. Discussion 15

6.1 Interpolation of φCO_2: GSA vs. sGs 15

6.2 Defining the multisource nature of CO_2 15

6.3 Rotokawa $\delta^{13}C_{CO2}$ analysis 17

6.4 White Island $\delta^{13}C_{CO2}$ analysis 18

6.5 Soil Gas Emissions at Rotokawa 18

6.6 A sulfur budget for Rotokawa 19

6.7 White Island CO_2 emissions 20

6.8 Heat flow from CO_2 emissions 21

6.9 Rotokawa: Structural and permeability controls on CO_2 emissions 22

6.10 White Island: Structural and permeability controls on CO2 emissions 24

7. Conclusions 24

8. Acknowledgements 26

9. References 26

10. Tables 34

11. Figures 36

Future Work 47

1. Soil gas surveys as a method for quantifying CO_2 emissions 47

2. Estimates for the TVZ from soil gas data 48

3. Tables and Figures **48**

Appendix 1 50

SEAWATER INFILTRATION AT WHITE ISLAND, BAY OF PLENTY, NEW ZEALAND: USING STABLE ISOTOPES OF CO2 AND H2O TO EVALUATE THE FLUID FLOW DYNAMICS **50**

1. Introduction **51**

1.1 Geological Setting 51

1.2 Origin of the fluids 51

2. Methods **52**

2.1 Soil gas and surface water sample collection 52

2.2 Stable Isotopic analysis 53

3. Results **53**

3.1 Isotopic analysis of soil CO2 53

3.2 φCO2 vs. $\delta^{13}C_{CO2}$ 54

3.3 Surface water analysis 54

4. Discussion **54**

4.1 $\delta^{13}C$ analysis of DIC and Flux 54

4.2 Evaluation of fluid flow dynamics 55

5. Conclusion **56**

6. References **56**

7. Tables **58**

8. Figures **59**

Appendix 2 64

DATA REPOSITORY

List of Tables

Table 1: *Results from GSA analysis of the raw data and sGs modelled data at RK* **34**

Table 2: *Results from GSA analysis of the raw data and sGs modelled data at WI* **35**

Table 3: *CO_2 emissions for four geothermal fields in the TVZ* **48**

Table 4: *Results from the soil gas flux, composition and temperature survey at WI* **58**

Table 5: *Isotopic composition of WI surface waters* **58**

List of Figures

Figure 1: *Field locations within the TVZ, and sampling locations within each field* **36**

Figure 2: *Plots of Soil Temperature vs. φCO_2 and $\delta^{13}C_{CO2}$ at RK and WI* **37**

Figure 3: *Histograms and variograms from the raw data of RK and WI* **38**

Figure 4: *Cumulative probability plot for RK* **39**

Figure 5: *Cumulative probability plot for WI* **40**

Figure 6: *Plots of $\delta^{13}C_{CO2}$ vs. φCO_2 and Cumulative probability for RK* **41**

Figure 7: *φH_2S vs. φCO_2 at RK* **42**

Figure 8: *Plots of $\delta^{13}C_{CO2}$ vs. φCO_2 and Cumulative probability for RK* **43**

Figure 9: *Pixel plots of the sGs modelled φCO_2 and soil temperatures at RK* **44**

Figure 10: *Pixel plots of the sGs modelled φCO2 and soil temperatures at RK* **45**

Figure 11: *International comparison of normalised and total CO_2 emissions* **46**

Figure 12: *Total CO_2 emission vs. Heat flow in the TVZ* **49**

Figure 13: *Map of Sampling at WI* **59**

Figure 14: *Plot of $\delta^{13}C_{CO2}$ vs. φCO_2 from soil gas in the crater floor* **60**

Figure 15: *Plots of $\delta^{18}O$ vs. δD of crater floor surface waters* **61**

Figure 16: *Crater floor isoscape of $\delta^{13}C_{CO2}$ and $\delta^{13}C_{DIC}$* **62**

Figure 17: *2d Schematic of the WI magma-hydrothermal system* **63**

Prologue

This thesis represents a significant body of work, detailing the heat and mass flow assessment of two magma-hydrothermal systems using soil gas flux surveys. The thesis objectives were laid out at the beginning of the study as:

1) Define a Total Soil CO_2 flux value for White Island using soil surveys within the crater floor.
2) Define a total CO_2 Mass value for Rotokawa geothermal field using soil gas flux surveys
3) Investigate graphical and isotopic techniques to differentiate magmatic, biogenic and atmospheric CO_2 in our field areas
4) Calculate Total heat and mass flow values for both field sites using existing or new geochemical data.
5) Investigate the fluid flow pathways and structural controls governing the surface expression of diffuse soil gas fluxes

Chapter 1: "Soil CO_2 emissions as a proxy for assessment of heat and mass flow, Taupo Volcanic Zone, New Zealand", will deal with these objective entirely, and composes the bulk of the work for the thesis. Chapter 1 is set to be submitted to G^3: Geochemistry, Geophysics, Geosystems. After analysing the results of the surveys at White Island, a sixth objective came out of the data:

6) Investigate the component sources of the soil gas released in the magma-hydrothermal system within the crater floor of White Island for clues into the nature of the shallow-subsurface permeability structures.

This objective is addressed in Appendix 1: "Seawater infiltration at White Island, Bay of Plenty, New Zealand: Using Stable Isotopes of CO_2 and H_2O to evaluate the fluid flow dynamics". This section will be formalised into a paper and be submitted in the future.

Chapter 1

Soil CO_2 emissions as a proxy for assessment of heat and mass flow, Taupo Volcanic Zone, New Zealand

[1*]Bloomberg, S, [2]Rissmann, C., [3]Mazot, A., [4]Werner, C., [1]Horton, T., [1]Oze, C., [1]Gravley, D., and [1]Kennedy, B.

[1]University of Canterbury, 20 Kirkwood Avenue, Ilam 8041, NZ

[2]Environment Southland, 202 Price Road, Waikiwi 9810, NZ

[3]GNS Science, 114 Karetoto Road, Wairakei 3377, NZ

[4]Alaska Volcano Observatory, 4200 University Drive, Anchorage, AK

[*]E-mail: simonhbloomberg@gmail.com

Contributions:

Mr. Bloomberg conducted the literature review, undertook the field work, geospatial mapping and wrote the manuscript. Dr. Rissmann conceived the study, assisted the field work , trained Mr. Bloomberg in CO_2 flux methodologies, geospatial mapping and geostatistical analysis. Dr. Mazot assisted the fieldwork and patiently trained Mr. Bloomberg in CO_2 flux methodologies and provided insight and guidance throughout the field seasons. Dr. Werner contributed unpublished data and reviewed the manuscript. Dr. Horton analysed the soil gas samples for stable isotopes of carbon and reviewed the manuscript. Dr. Oze, Dr. Gravley, and Dr. Kennedy provided reviews of the manuscript and good conversation at the pub. Special thanks also goes to Karen Britten (GNS Science) and Jo Pawson (UC) for assisting with fieldwork. This manuscript benefited greatly from endless reviews from the co-authors and Mighty River Power Ltd. Reviewers Tom Powell and Jeff Winick.

1. Abstract

The quantification of the heat and mass flow between deep reservoir(s) and the surface is a significant challenge to the sustainable development and exploration of magma-hydrothermal systems. Here, we use high resolution measurement of carbon dioxide (CO_2) flux and heat flow at the land surface to characterize the mass (CO_2 and steam) and heat released from the magma-hydrothermal systems. Statistical and isotopic characterization of background sources of CO_2 flux is utilized to reduce the level of uncertainty when deriving mass (emissions) and heat flow estimates from high temperature reservoirs. Soil gas and heat flow surveys at Rotokawa and White Island in the Taupo Volcanic Zone, New Zealand, include over 3,000 direct measurements of CO_2 flux, soil temperature, and soil gas carbon isotopes. Results indicate a total CO_2 emission rate of 633 ± 16 t d^{-1} (2.5 km^2) for Rotokawa and a total CO_2 emission rate of 116 ± 2 t d^{-1} for the crater floor (0.3 km^2) at White Island. Combining the magmatic-hydrothermal sourced CO_2 emission (constrained using stable isotopes) with reservoir H_2O:CO_2 concentration ratios and the enthalpy of evaporation, the thermal energy release for Rotokawa and White Island is 314 MW_t and 54 MW_t, respectively. CO_2 emissions are higher than previously published values by up to 570 td^{-1} at Rotokawa and 15 td^{-1} at White Island. Paired assessment of the CO_2 source using stable isotopes and statistical analysis of the CO_2 flux has reduced the uncertainty when constraining the magma-hydrothermal CO_2 emission from the reservoirs and has implications for blind geothermal system exploration

.

2. Introduction

Heat and mass transfer through magmatic-hydrothermal systems in the Taupo Volcanic Zone (TVZ) of New Zealand has been evaluated using a variety of surface geophysical, geochemical and geological techniques (*Donaldson & Grant,* 1978; *Lyon & Hulston*, 1984; *Bibby et al.*, 1995b; *Seward & Kerrick,* 1996; *Rowland & Sibson*, 2004). Surveys of magmatic-hydrothermal emissions are used to (1) better quantify the contribution of emissions to the global carbon cycle (cf. *Seward & Kerrick,* 1996; *Mörner & Etiope*, 2002), (2) identify temporal changes for volcano monitoring purposes (*Chiodini et al.*, 1998, 2005, 2008; *Brombach et al.*, 2001; *Frondini et al.*, 2004; *Werner et al.*, 2004a; *Mazot et al.*, 2011) and (3) assess the potential for geothermal power. As the measurement of CO_2 flux and its use as a proxy for total heat and total mass transfer has improved, the technique now has applications in geothermal exploration and field management (*Sheppard et al.*, 1990; *Werner et al.*, 2004b; *Bergfeld et al.*, 2006; *Fridriksson et al.* 2006; *Werner & Cardellini*, 2006; *Werner et al.*, 2008b; *Dereindra & Armannsson*, 2010; *Viveiros et al.* 2010; *Rissmann et al.*, 2011, 2012).

Magmatic-hydrothermal systems can be divided into non-volcanic and volcanic types (*Kerrick,* 2001; *Mörner and Etiope*, 2002). The CO_2 emission from actively degassing volcanoes (i.e. Vulcano; *Chiodini et al.*, 1998) is variable over a wide range of magnitudes. Diffuse degassing of non-volcanic systems (i.e. Reykjanes; *Fridriksson et al.*, 2006), when properly constrained, produces a similar range of emissions to active volcanoes or in some cases higher emissions as exemplified in New Zealand (cf. *Seward & Kerrick,* 1996; *Werner et al.*, 2004a & 2004b; *Werner & Cardellini*, 2006; *Rissmann et al.*, 2012). As such, when calculating total CO_2 emissions for convergent plate boundary volcanism (like the TVZ), inclusion of non-volcanic systems can only improve the accuracy of these carbon-cycle fluxes.

Here we compare high resolution soil gas flux and heat flow surveys for Rotokawa (RK), a developed high temperature (>200°C) non-volcanic geothermal system, and White Island (WI), an active andesitic stratovolcano, both within the TVZ. In addition to emission estimates, we also determined the sources of CO_2 at RK and WI using cumulative probability plots and stable isotopic analysis of ^{13}C and by comparison with CO_2 flux and soil temperature. Total heat flow (MW_t), total mass flow (Kg s^{-1}) and soil gas emission rates (t d^{-1}) are quantified for each survey along with detailed maps of the spatial extent and magnitude

of soil gas flux and heat flow. Normalized to total thermal area and total emission rates are contrasted with values reported for fields within the TVZ and worldwide (*Mörner and Etiope,* 2002*; Werner and Cardellini,* 2006*; Rissmann,* 2010*; Inguaggiato et al.,* 2012) and spatial maps of surface flux and heat flow are used to infer structural controls to fluid flow. Finally, a comparison is made between the observed CO_2 and derived heat flow estimates from this study and previously published estimates.

3. Geological Setting

3.1 Rotokawa (RK)

The geothermal system at RK fits within an 18-26 km^2 resistivity boundary defined by surveys completed in the 1960's and 1980's (*Hedenquist et al.,* 1988). The principal thermal feature is a warm (~24°C, surface) acid (pH ≈2.2) lake (Lake Rotokawa) with an area of ~0.62 km^2. To the north of the lake lies the RK thermal area with numerous thermal features (steaming ground, hot pools, sink holes, sulfur banks, hydrothermal eruption craters and fumaroles; *Krupp & Seward,* 1987). *Collar and Browne* (1985) noted that the hydrothermal explosions craters are less than 20,000 years old and structurally aligned in a NE/SW orientation coincident with deep field faults (*Winick et al.,* 2011). The RK thermal area has been extensively modified by historic sulfur mining and thermal features have been created where the land surface was excavated and/or a confining impermeable cap removed.

Two geothermal power stations generate from the geothermal reservoir (Figure 1), Rotokawa A (34MW_e) and Nga Awa Purua (140 MW_e). The maximum fluid temperature is ~320°C, recorded within the Rotokawa andesite deep reservoir rock (*Hedenquist et al.,* 1988). A two-phase fluid flows from the deep reservoir through to the surface along a deep field fault and mixes in a shallow aquifer near the lake (*Winick et al.* 2011). A local confining layer (a volcaniclastic lake deposit rich in clays, 'the Huka Falls Formation') has been removed in the thermal area by both hydrothermal eruptions and dissolution, this has opened the permeability for mixed neutral chloride and acid sulphate fluid to flow through hot springs and steaming ground (*Krupp & Seward*, 1987).

3.2 White Island (WI)

White Island (Whakaari) is an active andesitic stratovolcano located 50 km to the northeast of Whakatane, on strike with the eastern edge of the TVZ. The volcano is one of New Zealand's most active volcanoes over historic times; recent activity has been phreatic, phreatomagmatic and magmatic (*Houghton and Nairn,* 1991; *Cole et al.*, 2000; *Wardell et al.*, 2001). The gas chemistry is typical of active arc volcanism (*Giggenbach*, 1995).

The lithology of the crater floor is comprised of volcanic sediments and ash from eruptions, a landslide unit in the form of hummocks, and ancestral crater lake deposits (*Houghton and Nairn*, 1991). The only vascular life forms occur on the seaward flanks of the volcano but there is microbial activity within the crater floor soils and waters (*Donachie et al.*, 2002; *Giggenbach et al.*, 2003). These bacteria (i.e. methanogens) facilitate precipitation of minerals and produce CH_4 and CO_2 (*Castaldi and Tedesco*, 2005). Thermal features include steaming vents, active fumaroles (100-150°C; *Werner et al.*, 2008a), acid streams and pools, and steaming and boiling mud pots and pools. The western crater is filled with a large boiling acid lake (pH ≈ -0.2) demarking the center of modern day volcanic activity. Subsurface permeability at WI is mainly controlled by prescence/absence of hydrothermally-altered clay. Areas of high permeability create diffuse degassing structures and are often linked with landslide hummocks that have in-filled the crater floor during historic eruptions. Fumarolic activity has been monitored for the last 50 years (*Giggenbach* 1975a, 1975b, 1987; *Rose et al.* 1986; *Marty and Giggenbach, 1990; Giggenbach and Matsuo, 1991; Werner et al.*, 2008a).

4. Methods & Materials

4.1 Soil gas flux and temperature measurements

Soil gas flux (φ) surveys and subsoil gas sampling for compositional analysis of fumarolic gases were utilized to evaluate subsurface structural controls regulating fluid/gas flow to the surface. Soil gas flux of CO_2 (φCO_2) and H_2S (φH_2S) and soil temperatures were measured in the thermal areas at RK and at locations within the WI crater floor. The accumulation chamber method was used for assessing φCO_2 (*Chiodini et al.*, 1998; *Werner et*

382 *al.,* 2000; *Lewicki et al.,* 2005; *Rissmann et al.,* 2012). φCO_2 was measured using a West
383 Systems accumulation chamber and LICOR LI-820 infrared gas analyser for CO_2 (*Welles et*
384 *al.,* 2001) that is calibrated annually and has a sensitivity range of 0-20,000 ppm. *Evans et al.,*
385 (2001) and *Giammanco et al.* (2007) both tested the accuracy of the accumulation chamber
386 technique with a series of replicate measurements of known CO_2 effluxes through a synthetic
387 soil. *Evans et al.* (2001) found that the accumulation chamber measured a mean flux at -
388 12.5% below the imposed fluxes while *Giammanco et al.* (2007) reported an average
389 measurement error of ±5% that they attributed to natural variability, and recorded a mean
390 difference between measured and imposed fluxes of +5%. We used an identical system to
391 that assessed by *Giammanco et al.* (2007) and assume a similar mean measurement error of
392 approximately +5%. The fieldwork was undertaken in dry and stable conditions in order to
393 minimize the influence of rain, wind, soil humidity and atmospheric pressure changes on
394 φCO_2. Sampling of H_2S flux was limited at times due to the poor response of the chemical
395 sensor. Additionally, the purge time (<2 min) between consecutive measurements did not
396 enable the H_2S sensor to recover from previous high measurements. Due to the limited φH_2S
397 measurements, 'flux' in this study relates to φCO_2 unless otherwise stated.

398 Soil temperatures were measured to 10 cm depth within ~0.1m of the accumulation
399 chamber footprint using a Yokogawa TX-10 digital thermometer and a K-type thermocouple
400 (measurement accuracy ±0.5°C). Ambient air temperature and barometric pressure were
401 logged at the start of each day and after each 25 consecutive measurements of flux and soil
402 temperature. The flux survey design at RK used a systematic sampling approach (quasi-
403 regular grid spacing of 10 m - 25 m) coupled with an adaptive cluster component (e.g.
404 *Thompson,* 1990). Deviation from the systematic sampling pattern was guided by sensory cues
405 such as ground alteration and odour with the adaptive component initiated when a
406 measurement exceeded the estimated background flux level (>90 g m^{-2} d^{-1}, ≥ ambient T°C) at
407 which point the resolution increased to 5 m spacing. Due to time constraints at WI,
408 measurements were based on the systematic sampling approach only (Figure 1).

409 Two fumaroles were sampled at RK to find the H_2O:CO_2:H_2S concentration in steam.
410 They were sampled using the same setup from Rissmann (2010) and analysed in the same
411 laboratory.

412

4.2 Carbon isotopic analysis of soil gas

In order to define the magma-hydrothermal source, we analyzed the stable isotopic composition of CO_2 ($\delta^{13}C_{CO2}$) by collecting a gas sample concurrently with soil gas flux measurements in the West Systems accumulation chamber. A 5 mL syringe was used to pierce a rubber septum on top of the chamber. A gas sample was drawn and emptied into a helium filled 10mL exetainer vial capped with a pierceable butyl rubber septum. A fresh needle and syringe is used for each sample. Samples were taken direct from the chamber to prevent mixing and contamination from other possible sources of CO_2 (*Chiodini et al.,* 2008).

Values of $\delta^{13}C_{CO2}$ were determined using a Thermo Scientific GasBench II connected to a Delta V Plus gas isotope ratio mass spectrometer under continuous flow conditions within 48 hours of collection of the soil gas CO_2. A total of 60 samples at RK and 60 samples at WI were analysed. Stable oxygen and carbon isotopic compositions are accurate to <0.10 ‰ based on replicate analysis of NBS-19 and NBS-22 certified reference materials.

4.3 Data Analysis

Raw φCO_2 and φH_2S data were converted from ppm s^{-1} to g m^{-2} d^{-1} to account for the ambient temperature, atmospheric pressure and the area and volume of the accumulation chamber. Additionally, raw soil temperature values were converted from °C to W (watts) m^{-2} (following the procedure discussed in the next section).

Interpolation of the unsampled area was modelled using the sequential Gaussian simulation (sGs) algorithm within the WinGsLib software toolbox (*Deutsch & Journel,* 1998), and following the methods of *Cardellini et al.* (2003). The direct measurement data sets for φCO_2 and soil temperature/heat flow (Figures 2a & b) were declustered to remove the sample bias induced by using adaptive clustering and then normally scored prior to interpolation. Each simulation ran for 500 realisations at 10 m cell size using variogram models (Figure 3c & d). Post-processing of the 500 flux grid realizations included computation of mean flux and the probability of high and low fluxes at each location. Emission rates (t d^{-1}) for each realization were calculated by summing the simulated flux across the grid and multiplying by the grid area using the back-transformed data. The mean and standard deviations of the emission rates were computed from the 500 flux realizations conducted for each grid area.

CO_2 flux and soil temperature models were mapped as 2D pixel plots obtained from a pointwise linear averaging of the 500 realizations (E-type estimation) of each site. Finally, 2D pixel plots of the different flux populations were modeled using various flux cut-offs, set according to the population thresholds identified from isotopic values and log cumulative probability plots of φCO_2. The spatial distribution in soil temperatures were also modeled spatially through 500 sGs realizations using the method described for soil CO_2 flux.

As diffuse CO_2 flux from the soil may originate from multiple sources (i.e. soil-respired, atmospheric, and/or magmatic), flux data was evaluated using *Sinclair's* (1974) method by: 1) plotting geochemical data on a log-normal probability plot with a Gaussian distribution (cumulative probability) and 2) then separating the dataset into populations. Log cumulative probability plots were also applied to $\delta^{13}C_{CO2}$ and φCO_2, respectively, in attempt to better resolve the contribution of soil-respired or background sources to the total CO_2 emission occurring at both RK and WI (Figures 4 and 5).

The Graphical Statistical Approach (GSA) of *Chiodini et al.* (1998) is based on log cumulative probability plots of flux data and can be used to estimate total emissions. This was accomplished by summing the emission per population (E_i) which is calculated by multiplying the mean (M_i) CO_2 flux of each population (where "*i*" stands for each population recognized by cumulative probability plots) by S_i, the corresponding surface area (i.e. $E_i=M_i(S_i)$). An evaluation of S_i is obtained by multiplying the surface (S) of each study area (RK or WI) by the corresponding proportion (f_i) of the population (i.e., $S_i = f_iS$). The total CO_2 output from each site results from the summation of each population contribution. The central 95% confidence interval of the mean is used to calculate the uncertainty of the total CO_2 output estimation for each population.

4.4 Heat and mass flow from soil temperature

Soil temperature measurements were taken at RK (2914) and WI (690) at a depth of ~10cm. If the boiling point temperature (RK=98.7°C, WI=100°C) was reached before 10cm this was noted. Soil temperature measurements were converted to equivalent heat flow values using soil-temperature heat flow functions (Equations 1 and 2; Dawson, 1964). Dawson (1964) derived these equations from the relationship between surface heat flow (W m-2) and soil temperature at 15 cm depth at the Wairakei geothermal field. Broadly similar parent

materials and climatic conditions exist at RK and WI and therefore it is assumed that both formulas can be applied without change. Due to 80% of temperature measurements being recorded at the shallower depth of 10 cm we expect the converted heat flow values to be underestimates. Hochstein and Bromley (2005) found a diurnal variation of between 1-3°C at a depth of 10cm at the Karapiti thermal area, due to this minimal variation no diurnal temperature correction was applied to the soil temperature data.

Where soil temperature was below boiling point at 15 cm, Equation (1) is applied:

$$q_s = 5.2 \times 10^{-6} t_{15}^4 \quad (1)$$

where t_{15} is the soil temperature at 15cm depth and q_s is the soil heat flux in Wm^{-2}.

At sites where soil temperature exceeded boiling point at a depth (d_{BP}) of 10 or 15 cm, Equation (2) was applied:

$$q_s = 10^{\left(\frac{(\text{Log } d_{BP} - 3.548)}{-0.84}\right)} \quad (2)$$

From the transformed soil temperature data heat flow was simulated across each field using the sGs method as described above for CO_2. Total heat flow (MW_t) for each field was then computed by summing the simulated heat flow across the grid and multiplying by the grid area using the back-transformed data. The mean and standard deviations of the heat flow rates were computed from the 500 realizations conducted for each grid area.

Steam mass flow through the soil (F_{S,H_2O} in Kg s^{-1}) for each study area was approximated from heat flow values using the equation of Fridriksson et al. (2006):

$$F_{S\,(H_2O)} = \frac{H_S}{(h_{s,100°C} - h_{w,t_r})} \quad (3)$$

where H_s is the calculated heat flow in Watts from Equations (1) and (2), $h_{s,100°C}$ is the enthalpy of steam at 100°C (2676 kJ/kg) and h_{w,t_r} is the enthalpy of water at the mean annual temperature for the field areas (RK=23°C;96kJ/kg, WI=10°C:41.9kJ/kg; *NIWA.co.nz,* 2011*;* *Schmidt and Grigull,* 1979).

4.5 Heat and mass flow and emissions calculations from CO_2 flux

An alternative measure of the steam mass flow (or heat release) from the high temperature reservoirs at both fields is made by multiplying the total CO_2 emission rate by the representative concentration ratio of CO_2 in steam (H_2O:CO_2) supplying surface thermal activity (*Chiodini et al.,* 2005; *Fridriksson et al.*, 2006):

$$F_{stm(CO_2)} = F_{CO_2} . \frac{[H_2O]}{[CO_2]} \quad (4)$$

where F_{CO_2} is the total flux of CO_2 in g s^{-1}, $\frac{[H_2O]}{[CO_2]}$ is the concentration ratio in g, and $F_{stm(CO2)}$ is the steam mass flow in g s^{-1}. In this way we can calculate the quantity of steam mass flow that is condensed within the subsurface by comparing Fstm(CO_2) with the value from heat flow through soil ($F_{s\,(H_2O)}$), Equation (3), *Fridriksson et al.,* 2006).

An equivalent heat flow (H_s) can be calculated for the steam mass flow ($F_{stm(CO2)}$) derived from Equation (4) using:

$$Hs = F_{stm(CO_2)} . h_{s,100°C} \quad (5)$$

where Fstm(CO_2) is from Equation (4), and is the steam flux in g s^{-1}, and $h_{s,100°c}$ is the enthalpy of steam at 100°C (2676 kJ/kg) and Hs is the heat flow in Watts (*Fridriksson et al.*, 2006).

5. Results

5.1 Rotokawa: Diffuse soil gas fluxes, stable isotopes and soil temperatures

Diffuse soil CO_2 fluxes range from <1 to 127,808 g m^{-2} d^{-1} from 2,914 direct measurements (Figure 2a). Across a 1.4 km^2 area of the RK field the arithmetic and declustered means were 1146 g m^{-2} d^{-1} and 234 g m^{-2} d^{-1}, respectively, while the sGs produced a mean of 246 g m^{-2} d^{-1}. Twenty six per cent of the raw fluxes were greater than 100 g m^{-2} d^{-1} and less than 10% were greater than 1000 g m^{-2} d^{-1} (arbitrary bins). The coefficient of variation is 8.4 with the population being approximately log-normal with a positive skew which is consistent with a CV >1 for non-normal data (Figure 3a). Raw (GSA) and sGs total CO_2 emission estimates were 1727 and 353 t d^{-1} for the 1.4km^2 modeled area (Table 1).

Shallow soil temperatures (Figure 2a) ranged from 9 °C to boiling point (98.7°C at 350m ASL.). The arithmetic and declustered means were 29.5 and 23.4 °C. In terms of high temperatures, 10% of the data had temperatures > 50 °C and < 2% of the data was within error of boiling point (± 0.5 °C). The relationship between CO_2 and soil temperature at RK has an r^2 value of 0.26.

$\delta^{13}C_{CO2}$ values (‰) range from -16.5 to -7.3 (n=60). The relationships between $\delta^{13}C_{CO2}$ with soil temperature (Figure 2a) and φCO_2 (Figure 6) at RK have an r^2 value 0.08 and 0.3, respectively. The $\delta^{13}C_{CO2}$ values of the CO_2 flux at RK can be split into those areas of flux >1,000 g m^{-2} d^{-1} with a mean of -8.5 ± 0.4 ‰ and areas of flux <1,000 g m^{-2} d^{-1} with a mean of -10.3 ± 0.5 ‰. The mean for the whole dataset is -9.7 ± 0.4 ‰.

554 ***5.2 Rotokawa: φH2S and relationships with φCO2***

555 Samples of φH_2S from 121 sites range from 0.2 to 156 g m^{-2} d^{-1}. The r^2 value for CO_2
556 and H_2S is 0.65 (Figure 7) though for H_2S and soil temperature it is 0.25. In Figure 7 we plot
557 the fluxes comparatively and find a threshold relationship where φH_2S is below detection
558 until φCO_2 values exceed a threshold of ~100 g $m^{-2}d^{-1}$ at which point both gaseous species
559 are detected.

560 Two fumarole samples were used to calculate the CO_2:H_2S ratio of surface advective
561 steam flow (pipe flow). The range of the ratios (Figure 7) provides an estimate of the
562 distribution of the gas composition for advective degassing. While a few of the soil fluxes fall
563 within this range most of the data show a higher CO_2:H_2S gas flux ratio.

564 The CO_2:H_2S ratio for the fumaroles has a mean of 7.9 while the mean ratio for
565 significant soil gas flux is 241, historic gas data from wells puts the ratio around 45
566 (*Hedenquist et al.* 1988).

567

568 **5.3 White Island: Diffuse soil gas fluxes, stable isotopes and soil temperatures**

569 Fluxes range from <1 to 29,896 g m^{-2} d^{-1} from 691 direct measurements (Figure 2b)
570 with an arithmetic and declustered mean of 619 ± 80 g m^{-2} d^{-1} and 367 ± 40 g m^{-2} d^{-1}. Of the
571 raw fluxes, 44% were greater than 100 g m^{-2} d^{-1} and 10% where greater than 1000 g m^{-2} d^{-1}.
572 The coefficient of variation is 3.2 with the total population being approximately log-normal
573 with a positive skew which is consistent with a CV >1 for non-normal data (Figure 3b). The
574 raw (GSA) and sGs total CO_2 emission rates were modeled for the crater floor (0.31 km^2) of
575 240 ± 4 t d^{-1} and 116 ± 2 t d^{-1}, respectively (Table 2).

576 Shallow soil temperatures (Figure 2b) ranged from 15 °C to boiling point (100°C).
577 The arithmetic and declustered means were 40.3 and 37 °C. In terms of high temperatures,
578 19% of the data had temperatures > 50 °C and < 2% of the data was within error of boiling
579 point (± 0.5 °C). The relationship between CO_2 and soil temperature at has an r^2 value of
580 0.27.

581 $\delta^{13}C_{CO2}$ values (‰) range from -12.5 to -1.4 (n=60, Figure 8). The $\delta^{13}C_{CO2}$ values of
582 the CO_2 flux at WI can be split into those areas of flux >1000 g m^{-2} d^{-1} with a mean of -1.9 ±
583 0.3 ‰ and areas of flux <1000 g m^{-2} d^{-1} with a mean of -7.6 ± 0.5 ‰. The mean for the whole

584 dataset is -5.8 ± 0.8 ‰. Plotting $\delta^{13}C_{CO2}$ vs. soil temperature (Figure 2b) and CO_2 (Figure 8)
585 produces r^2 values of 0.71 and 0.78.

586

587 **5.4 Heat and mass flow based on soil temperature measurements**

588 Using Equations 1 and 2, the data was modeled with sGs then converted to heat flow
589 in W m^{-2} and finally into a total megawatt (MW_t) value. For RK heat flow measurements
590 ranged between 0.03 – 4526 with a mean of 15 W m^{-2}. At WI this ranged from 0.28 – 4526
591 with a mean of 62 W m^{-2}. The total heat flow through soil is estimated to be 37 ± 1.5 MW_t at
592 RK and 19.5 ± 0.5 MW_t at WI.

593 The total heat flow through soil in watts can be used with Eq.3 to find the equivalent
594 steam mass flow (*Fs (H_2O)*). At RK and WI the surface heat flow values are equivalent to
595 1267 ± 23 t d^{-1} and 642 ± 10 t d^{-1} H_2O, respectively.

596

597 **5.5 Heat and mass flow calculated from CO_2 degassing**

598 Calculating the total heat input to RK was accomplished using Equations (4) and (5),
599 where the total magmatic-hydrothermal CO_2 flux (614 t d^{-1}, see discussion) is multiplied by
600 the H_2O:CO_2 ratio in the deep fluid (61g kg^{-1} or 1:16.6; *Hedenquist et al.* 1988), to give a
601 steam flux ($F_{stm(CO2)}$) of 10,204 ± 255 t d^{-1} H_2O. From this value a heat flow of 315 ± 8 MW_t
602 is calculated. Combining the 10,204 t d^{-1} H_2O and 615 t d^{-1} CO_2 equivalent to 125 ± 3 Kg s^{-1}
603 total mass flow which is in good agreement with previously published values for total mass
604 flow of 144 and 105 Kg s^{-1} (*Seward & Kerrick,* 1996; *Bowyer & Holt,* 2010).

605 At WI, the total magmatic-hydrothermal CO_2 emission (see discussion) of 114 t d^{-1} is
606 multiplied by the H_2O:CO_2 (159.5g kg^{-1} or 1:6.27; *Giggenbach & Matsuo*, 1991; *Werner et*
607 *al.*, 2008a), to give a steam mass flow ($F_{stm(CO2)}$) of 721 ± 10 t d^{-1} H_2O and a heat flow total of
608 22 ± 0.5 MW_t. We estimate a total island heat and mass flow using the normalized CO_2 flux
609 value for the crater diffuse degassing (230 t d^{-1}, 0.6 km^2) and the average plume emission
610 during the study period (1,000 ± 100 t d^{-1} CO_2, *geonet.org.nz,* 2012) of 1,230 ± 100 t d^{-1} CO_2
611 which converts to a heat flow of 238 ± 20 MW_t and a steam mass flow of 7,700 ± 600 t d^{-1} or
612 a total mass flow of 8900 t d^{-1} or 100 Kg s^{-1}.

6. Discussion

6.1 Interpolation of φCO_2: GSA vs. sGs

Interpreting and discussing the data collected and analyzed in this study for defining the source and emission of CO_2, total heat flow, and structural controls at WI and RK is dependent on the interpolation approach. The GSA allows the definition of a confidence interval, though it does not take into account the spatial correlation between the data, resulting generally in an overestimation of the uncertainty (*Cardellini et al.*, 2003). This affect is induced by sampling predominantly in the areas of thermal activity and thus biasing the raw data by having an over represented anomalous flux population. By assuming a solely statistical estimation, the GSA will not accurately represent any unsampled (in this case, non-thermal) areas. For that reason we report the sGs results and use them here for further analysis (Table 1 & 2). It is important to note that GSA is used in this study as a technique for assessing the natural distribution of CO_2 and heat flow data, and can be used in conjunction with other data to assess the origins of CO_2.

6.2 Defining the multisource nature of CO_2

In order to use total CO_2 emission values for the estimation of heat and mass flow from a magmatic-hydrothermal system it is necessary to define the contributions from the different φCO_2 sources. To produce these values, any contribution from non-magmatic-hydrothermal sources (background/atmospheric or soil-respired/biogenic in this case) must be removed from the calculation. Two methods were employed in this study: (1) the GSA method of breaking the flux data into populations and (2) the use of stable isotopic analysis of the φCO_2 to identify source components.

When using GSA, we assume that low flux populations (<30 g m^{-2} d^{-1}) are background for a system in which permeability is constant. The heterogeneity in permeability at our field sites and the large volume and pervasiveness of magma-hydrothermal φCO_2 population means this method, on its own, may not fully constrain the source populations. The latter became evident when stable isotope analysis was paired with flux data (Figures 4 and 5), and

643 there were fluxes which had magma-hydrothermal $\delta^{13}C_{CO2}$ values (filled circles, Figures 4
644 and 5) that had previously been in the low flux populations defined during the GSA. While
645 GSA does not fully constrain a source, it can illustrate the natural variations within the total
646 flux population, which makes it feasible as a method for the quick estimation of a source's
647 contribution. However, as noted by others the partitioning procedure does not result into a
648 unique solution (*Chiodini et al.,* 2008).

649 When *Chiodini et al.* (2008) first applied this method to finding the source populations;
650 GSA populations of the flux data were reduced into two partitions, a low and high flux group.
651 This meant that when they compared their isotopically partitioned populations to the GSA
652 populations, the GSA populations were found to have overestimated the limits of the
653 background flux populations significantly. In this study, the flux data was fully partitioned
654 using GSA in to 5 populations and then compared with the 3 isotopically partitioned flux
655 populations (Figures 4 and 5). An overestimation of the low flux GSA populations was not
656 produced, and the two different datasets produced similar thresholds for background fluxes.

657 While the GSA populations are defined by inflections in the slope and therefore span
658 defined sections of the total flux (Straight Lines, Figures 4 and 5), the stable isotope analysis
659 has provided source populations which in some instances span the whole range of fluxes
660 (Filled circles, Figures 4 and 5). The paired use of stable isotopes and GSA to isolate the
661 source populations is the method used in this study, as it was in *Chiodini et al.* (2008);
662 however, a complete analysis of the flux data using the paired assessment of sources led to
663 well-defined thresholds for constraining the magmatic-hydrothermal CO_2 emission.

664 Figures 4 and 5 show the cumulative probability plots of total flux at RK and WI with
665 populations from the GSA and from the stable isotopic analysis superimposed. Though these
666 methods differ in which variable is used to determine the component source, they combine to
667 produce values for the background or non-magma-hydrothermal contribution threshold. The
668 thresholds were set at <30 for RK and <25 g m^{-2} d^{-1} for WI. The thresholds were derived
669 from averaging the lightest isotopic population (Figures 4 and 5) which fits within the GSA
670 populations 1 & 2 (determined to be "background"). The value at WI is slightly higher than
671 the 15 g m^{-2} d^{-1} threshold found by *Werner et al.* (2004a) though their study used statistical
672 analysis to constrain the flux population.

673

6.3 Rotokawa $\delta^{13}C_{CO2}$ analysis

The maximum $\delta^{13}C_{CO2}$ of the φCO_2 (-7.3‰) is consistent with the findings of *Hedenquist et al.* (1988) for RK4 (gas phase CO_2 in the well, -7.9‰) and for the Rotokawa fumarole (vent, -7.8‰), and indicates that the deep carbon source is indistinguishable from the soil CO_2 samples taken within the thermal area. The contribution to soil CO_2 from different sources can be observed in Figure 6 where the maximum isotopic value of -7.3‰ is defined as the magmatic-hydrothermal end-member and the minimum value of -16.5‰ is the background end member. A large area of the thermal area at RK is vegetated by C3 plants (e.g. prostrate Manuka) which yield a $\delta^{13}C_{CO2}$ of -24‰ (*Amundson et al.,* 1998) during decomposition and root respiration. The other minor contributions to φCO_2 are from litter and humus decomposition and infiltration of the atmospheric CO_2, both of which minimally contribute if there is active root respiration occurring (*Amundson et al.,* 1998).

The average $\delta^{13}C_{CO2}$ value from the sampling at RK is -9.7 ± 0.4‰ though no spatial correlations can be drawn here due to the biased sampling design. In locations of hydrothermal-dominant CO_2 (>-9.9‰) we also find a good correlation with high φCO_2 (mean of 8000 g m^{-2} d^{-1}) while in areas of mixed sources (<-10‰) we find a mean φCO_2 of 114 g m^{-2} d^{-1}. High water tables can reduce anomalous soil temperatures while not affecting the flux (Figure 9a and b), therefore the correlation between soil temperature and $\varphi CO_2/\delta^{13}C_{CO2}$ are limited (Figure 2a).

In many areas of low flux (<100 g m^{-2} d^{-1}), $\delta^{13}C_{CO2}$ signatures (>-8‰, Figure 6) were relatively positive suggesting that permeability is constraining the soil gas flux of magma-hydrothermal CO_2, as opposed to the low fluxes from soil-respired or atmospheric CO_2 . For example, the lowest measured $\delta^{13}C_{CO2}$ signature is -16.5‰ and corresponds to a φCO_2 of 59 g m^{-2} d^{-1}. If the origin of the isotopically lightest soil-respired CO_2 is -24‰, then the -16.5‰ value is significantly mixed with hydrothermally-sourced CO_2. A flux of 59 g m^{-2} d^{-1} is at least 2 to 4 times as large as natural soil respired background (15 – 30 g m^{-2} d^{-1}) measured for un-irrigated pasture in the Taupo Volcanic Zone (pers. comm. Rissmann, 2012). This suggests a significant hydrothermal CO_2 input even at low flux sites (<100 g m^{-2} d^{-1}) and, therefore, the dominant control on flux is permeability. These types of correlations show that $\delta^{13}C_{CO2}$ measurements have profound implications for the discovery of blind geothermal systems concealed by low CO_2 fluxes.

705

706 **6.4 White Island $\delta^{13}C_{CO2}$ analysis**

707 The samples of soil CO_2 had a maximum $\delta^{13}C_{CO2}$ of -1.4‰ which is slightly more
708 positive than the vent samples by *Marty and Giggenbach* (max -2‰, 1990) but within error
709 of *Giggenbach and Matsuo* (max -1.5‰, 1991). The $\delta^{13}C_{CO2}$ samples measured at high flux
710 sites (>1000 g m^{-2} d^{-2}) are stable between the range of -1.4 and -2‰ (mean -1.9‰) which
711 matches those of the historic samples (Figure 8). This indicates that the magmatic-
712 hydrothermal source has been sampled and gives a value for the magma-hydrothermal
713 reservoir end-member.

714 Isotopically heavy signatures paired to high flux zones (>1000 g m^{-2} d^{-1}, Figure 8)
715 supports a magma-hydrothermal origin for the φCO_2. The highest fluxes measured in our
716 study are located along the central sub-crater's eastern rim (Figure 10a). The correlation of
717 the highest flux with the heaviest $\delta^{13}C_{CO2}$ is indicative of an area at depth where the greatest
718 amount of magmatic-hydrothermal CO_2 is released and fluids ascend rapidly to the surface
719 due to high permeability (*Werner and Cardellini,* 2006; *Rissmann et al.,* 2012).

720 The minimum value of -10.2‰ occurs at low φCO_2 of 12.5 g m^{-2} d^{-1}. The signature in
721 this case is significantly lighter than magmatic but heavier than any pure soil-respired
722 signature and the associated flux is considered low or background. Due to the total lack of
723 vegetation or soil development within the crater floor, the -10.2‰ value must be wholly
724 atmospheric CO_2 and/or from microbial respiration (i.e. methanogenesis) of CH_4 (where
725 $\delta^{13}C_{CH4}$ is ~22‰) which is abundant at WI.

726 The average value of $\delta^{13}C_{CO2}$ at WI is -5.8 ± 0.7‰ and indicates a saturation of the
727 soil with a mix of the magma-hydrothermal sourced CO_2 and input from background sources
728 (atmospheric and/or microbial respiration). In locations of magma-hydrothermal-dominant
729 CO_2 (>-4‰) we also find a good correlation with high φCO_2 (mean of 9,216 g m^{-2} d^{-1}) while
730 in areas of mixed sources (<-4 ‰) we find a mean φCO_2 of 86 g m^{-2} d^{-1}.

731

732 **6.5 Soil Gas Emissions at Rotokawa**

733 Soil gas flux measurements at RK geothermal field cover a wide range (<1 to 127,808
734 g m^{-2} d^{-1}) with a significant throughput of magmatic-hydrothermal CO_2 within regions of the

735 thermal ground. The mean for the total CO_2 population when compared with the background
736 removed total (246 vs. 1082 g m^{-2} d^{-1}) is significantly different. This is reconcilable with the
737 ground cover at RK which is heavily vegetated and indicative of minimal conductive heat
738 flow (i.e. western areas of Figure 9a) as well as shallow clays with low permeability reducing
739 the magnitude of flux (i.e. Figure 6).

740 The thermal area at RK is actually larger than the area modxeled in our study. For the
741 full thermal field (defined by resistivity and vegetation analysis, 2.5km^2), a minimum
742 emissions estimate is calculated by normalizing the emission rate by 1.4 km^2 (i.e., 8.99 x 10^4
743 t yr^{-1} km^2) and extrapolating to 2.5 km^2. Extrapolation provides an emission rate of 633 ±
744 16td^{-1}. This normalized emission rate is purely for soil zone CO_2 and does not include
745 measurement of gaseous efflux from any other thermal features at RK (Lake Rotokawa, hot
746 pools, fumaroles, mud pools). Applying the magmatic-hydrothermal CO_2 threshold to this
747 total emission value reduces the product to an emission of 614 ± 15 t d^{-1}.

748 The total CO_2 emissions at RK calculated from the sGs have produced a thermal area
749 normalised (89,963 t yr^{-1} km^{-2}) value that is one of the largest total CO_2 non-volcanic
750 emissions in New Zealand. The RK value is equivalent 350% of normalised emission for the
751 Rotorua geothermal system (25,426 t yr^{-1} km^{-2}; *Werner and Cardellini,* 2006) and 50% of the
752 normalised soil gas emissions of WI (139,916 t yr^{-1} km^{-2}; Figure 11). Historically,
753 measurements at RK indicated a small CO_2 emission; *Seward and Kerrick* (1996) calculated
754 a total CO_2 emission from RK to be ~55 t d^{-1} based on a total mass flow of 144 Kg s^{-1} and a
755 concentration ratio of kgH_2O:4.4gCO_2. This H_2O:CO_2 ratio was the key factor in their
756 underestimation of the CO_2 flux. The high spatial resolution of direct measurements in this
757 study has produced a similar total mass flow to the *Seward and Kerrick* (1996) value of 144
758 Kg s^{-1}; however, our CO_2 value of 614 ± 15 t d^{-1} indicates that the *Hedenquist et al.* (1988)
759 H_2O:CO_2 concentration ratio of kgH_2O:61gCO_2 is more accurate.

760

761

762 **6.6 A sulfur budget for Rotokawa**

763 In order to produce a sulfur budget, the CO_2 emissions associated with all fluxes in
764 excess of 100 g m^{-2} d^{-1} are multiplied by the molar CO_2:H_2S ratio for the soil zone to produce

765 a total H_2S emission from diffuse soil degassing of 2.6 t d^{-1}. Two previous study from Lake
766 Rotokawa found 84.3 and 10.4 t d^{-1} SO_4^{2-}, which equates to 29.9 and 3.67 t d^{-1} H_2S
767 (multiplying by the molar weight ratio, sulfur oxidation), respectively (*Krupp and Seward,*
768 1987; *Hedenquist et al.,* 1988; *Werner et al.,* 2008b). This gives a minimum total surface
769 sulfur emission for RK of 6 t d^{-1} with a minimum total emission of H_2S from the reservoir at
770 80 t d^{-1} (multiplying the total CO_2 by the CO_2:H_2S fumarole ratio). The loss of ~74 t d^{-1} of
771 H_2S within the subsurface is attributed to being scrubbed by shallow groundwater and/or
772 precipitates (as elemental S) before reaching the surface of the field. This can be reconciled
773 with the large (2.6 Mt) sulfur lode found within cm's of the surface at RK. At 6 t d^{-1} the lode
774 would take a minimum of 1150 years to accumulate or 100 years at 80 t d^{-1}. *Krupp and*
775 *Seward* (1987) estimated the deposit accumulated at 5 t d^{-1} over 1420 years which could
776 indicate that RK has been emitting similar rates of H_2S and, therefore, CO_2 for over 6,000
777 years. Due to the Taupo pumice alluvium capping the area these deposits are now at depth
778 and the current rate of deposition is greatly reduced and is spatially confined to lake
779 Rotokawa (*Krupp & Seward.,* 1987).

780 φH_2S occurs in background concentrations until φCO_2 becomes advective (Figure 9).
781 Based on interpretations of this phenomenon by *Werner et al.* (2008b) it is assumed that a
782 similar process is occurring at RK, where during low CO_2 fluxes, diffusion is the main
783 mechanism and H_2S is removed, but when there is high CO_2 flux some H_2S can reach the
784 surface.

785

786 **6.7 White Island CO_2 emissions**

787 The difference between the total mean φCO_2 and magmatic-hydrothermal mean φCO_2
788 for the crater floor diffuse degassing (368 vs. 723 g m^{-2} d^{-1}) indicates a significant area has
789 background emission which is consistent with the flux map (Figure 10a). The range of flux
790 values at WI, though not as broad as at RK, does have a higher mean value, which is an
791 indicator of the reduced contribution of background sources to the total gas emissions
792 through the crater floor (4% background at RK vs. 1.3% background WI). Removing the
793 background contribution to the emission gives a value of 114 t d^{-1}.

There are obvious flank and crater wall emissions at WI, so for the total island φCO_2 an area of 0.6 km^2 is multiplied by the normalized rate (1.39 x 10^5 t yr^{-1} km^{-2}) and gives 230 ± 3 t d^{-1} CO_2. This is a maximum total diffuse degassing emission for WI.

The value of 114 t d^{-1} or 10% of the total emission is consistent with the latest published study at WI by *Werner et al.* (2004a) who found an emission of 99 t d^{-1} and 10% of the total emission from 268 points (<1000 points/km^2). *Wardell et al.* (2001) found an emission of 10 t d^{-1} and <1% of the total emission, though their survey was less than 20 points (<100 points/km^2).

6.8 Heat flow from CO_2 emissions

For both RK and WI, measured soil temperature data was converted to equivalent heat flow using Equations (1) and (2), whereas, heat flow based on CO_2 emissions was calculated using Equations (4) and (5). Both RK and WI display lower observed heat flow than that estimated from CO_2 emissions. The discrepancies in heat flow values likely reflect the condensation of 88% (37 and 314 MW_t, RK) and 12.5% (19.5 and 22 MW_t, WI) of the steam phase within shallow groundwater that overlies the high temperature reservoirs.

Fridriksson et al. (2006) report the condensation of 87% of steam mass flow for the Reykjanes thermal area in Iceland as based on the discrepancy between observed heat flow and heat flow estimated from CO_2 flux, which matches closely with the discrepancy at RK. The system at RK probably loses more heat laterally (like Reykjanes) to cooler groundwater inflows triggering condensation of rising hydrothermal fluids, as well as having a deeper heat source (4-5km; *Winick et al.*, 2011). Conversely, WI probably loses less heat to the local groundwaters as the hydrothermal heat source is shallower (<1-2 km depth; *Cole et al.*, 2000; *Wardell et al.*, 2001; *Werner et al.*, 2008a) and there is a concentrated plume that only opens to lateral degassing at depths of <300m (*Werner et al.*, 2008a).

Historic heat flow studies at RK presented in *Hedenquist et al.* (1988) and *Seward and Kerrick* (1996) put the thermal energy release between 210 and 236MW_t but also report numbers as high as 600MW_t. *Bibby et al.* (1995b) estimated a total heat outflow for RK of 300 MW_t which is close to this study's value of 315 ± 8 MW_t. These historic values of heat flow are all based on chloride measurements, which might be less conservative when it

comes to fluid-rock interaction (*Bibby et al.*, 1995a) and is also less mobile than CO_2. For groundwater having reached saturation with respect to CO_2, the majority of the gas passes through to the surface. This relatively conservative behavior of CO_2 makes it a better proxy of heat release from the shallow reservoir than chloride or measurement of observable heat flow (*Chiodini et al., 2005; Rissmann et al.,* 2011). The main error associated with any CO_2 based estimate of reservoir heat release is the correct estimation of CO_2 emission and the selection of a representative molar H_2O:CO_2 ratio. At RK we used a high spatial resolution to reduce the uncertainty in the CO_2 emission, and the concentration ratio of 16.6 is considered representative (as discussed in Section 5.3) and therefore the value of 315 ± 8 MW_t is considered representative.

White Island's plume was assessed by *Giggenbach and Sheppard* (1989) as a proxy for the island's mass and heat flow and found that it depended on the state of volcanic activity. Quieter periods had steam plumes of 5000 t d^{-1} and 240 MW_t, and active periods had plumes of 18,000 t d^{-1} and 810 MW_t. These mass flows were derived using SO_2 flux measured aerially with COSPEC-V and H_2O:CO_2:SO_2 mole-ratios, which were higher ($kgH_2O/240gCO_2$) than the concentration of CO_2 in steam ratio used in this study (kgH_2O:$159.5gCO_2$; see Section 4.4). *Rose et al.,* (1986) found a steam degassing rate of 8000-9000 t d^{-1} which is similar to this study's value (7700 ± 600 td^{-1}). *Werner et al.* (2008a) described the H_2O:CO_2 ratios at WI as stable since a notable decrease in activity since 2000 and therefore the CO_2 concentration ratio of 159.5g kg^{-1} is considered a representative mean value and was used in this study to calculate a heat flow of 238 MW_t.

Our data indicates that high spatial resolution φCO_2 surveys are sufficient or superior for constraining the heat and mass flows of hydrothermal systems compared to other mechanisms such as, soil temperatures, chloride flux or SO_2 emissions.

6.9 Rotokawa: Structural and permeability controls on CO_2 emissions

Figure 9a shows the significant flux (>300 g m^{-2} d^{-1}) anomalies are quasi-circular in nature but become more diffuse and broadly distributed at lower flux rates. There is a clear correlation of surface thermal features with areas of high flux. Areas of thermal features are concentrated either along lineations that trend NE or within the bounds of historic hydrothermal eruption craters (Figure 9a). The highest flux values occur along the lake shore

855 and coincide with lower average soil temperatures (<50°C, Figure 2a) indicating some
856 decoupling of steam flow likely due to high water tables adjacent to the lake (Figure 9b). To
857 the north and northwest greater coupling between heat flow (high soil temperatures) and CO_2
858 flux indicates less scrubbing of the steam phase by cooler lake waters (Figure 9b). The active
859 thermal area has been mapped previously using resistivity boundaries and thermal anomalies
860 (*Gregg,* 1958; *Hochstein*, 1990) and the flux map does not produce any anomalous flux or
861 thermal anomalies outside of this mapped boundary.

862 The location of the thermal area at RK coincides with a series of historic
863 hydrothermal explosion craters. The largest of which is the site of Lake Rotokawa (*Collar*
864 *and Browne,* 1985). Vigorous surface thermal activity surrounds the explosion craters and
865 includes boiling acidic SO_4-Cl springs and steaming ground. Most diffuse degassing is
866 coupled to these thermal features and decreases rapidly in magnitude with distance away
867 from them. Of note there is a major anomaly along a feature attributed to a hydrothermal
868 eruption crater rim by *Krupp and Seward* (1987) which runs E-W for 300m across the
869 thermal area.

870 Lake Rotokawa, a depression caused by a hydrothermal eruption crater, has a large
871 recharge of CO_2-unsaturated meteoric waters to depths of >200m. This depth is enough to
872 dissolve any fluxing CO_2 and no visible bubbles are present mid lake. Close to the lake shore
873 it shallows steeply and so that water column can be saturated in CO_2 and any incoming flux
874 will degas at the surface as bubbles. Some of the highest measured φCO_2 is located close to
875 the shore line which is indicative of significant permeability related to the rim of a large
876 hydrothermal eruption crater (*Collar & Browne,* 1985; *Krupp and Seward,* 1987).

877 Historic mining of sulfur has also affected the topography of the thermal area by
878 creating depressed surfaces which now intersect with the water table allowing hot springs and
879 steaming ground to form.

880 Deep field faulting can cause hot spots of high permeability that allows boiling fluids
881 to rise (*Fairley and Hinds,* 2004; *Rowland and Sibson,* 2004; *Heffner and Fairley,* 2006;
882 *Rissmann et al.,* 2011). There is a large field fault running through the middle of the RK
883 thermal area, the Central Field Fault (CFF, Figure 9a) of *Winick et al.* (2011), which indirectly
884 influences the diffuse degassing structures with historic eruptions craters that appear to focus
885 thermal activity, occurring along its strike. The magnitude of the gas fluxes in the vicinity of

these craters and along the strike of the CFF suggests a deep-seated connection between surface eruption craters and the CFF which is likely channeling fluids from depth.

6.10 White Island: Structural and permeability controls on CO2 emissions

The hydrothermal system at WI is actively degassing through permeable areas of the crater floor, we show a correlation with surface thermal feature such as mounds and areas around fumaroles, historic crater margins, and breaks in slope (Figure 10a & 10b). The mounds host numerous small fumarolic vents that are encrusted with sulfur condensate, are of high temperature, and comprised of highly altered clays, all of which makes them analogous to the diffuse degassing structures (DDS) characterized by *Chiodini et al.*, (2005). The vigor, size and number of DDS along with steaming ground and acidic-Cl outflows increases with proximity to the Crater Lake and the modern day center of volcanic activity.

Most of the total CO_2 emission is exhausted through the Crater Lake (*Werner et al.*, 2008a) and around its rim there is a high flux zone. In the middle of the crater floor there is an arcuate channel of high flux and high temperatures that aligns closely with an old crater rim (Figure 10a & b). This area is one of the most permeable at WI, with boiling mud pots and steaming ground common, this disproportionate flow of heat and mass is evidence of a connection at depth as has been suggested by *Houghton and Nairn* (1991) and *Giggenbach et al.* (2003). Diffuse degassing, fumaroles, and steaming ground are present at breaks in slope (crater floor/wall, crater wall/rim, crater floor/mound) which are generally places of deposition or erosion, so strata would likely have high permeability as it is less lithified.

Elsewhere on the island there are areas of capping clays at around 1m depth that limit degassing locally. These are hypothesized to be the remnants of the old crater floor/lake Hope (*Giggenbach et al.*, 2003), consisting of impermeable and altered volcaniclastic material.

7. Conclusions

1) The hydrothermal systems and their respective surface thermal expressions at RK and WI emit an extraordinary quantity of CO_2 and thermal energy per unit area. This study continues with the style and approach of recent soil gas surveys at New Zealand geothermal systems (Rotorua, *Werner & Cardellini*, 2006; Ohaaki, *Rissmann et al.*, 2012) which couples the use of interpolation (sGs) and extrapolation of φCO_2 in order to estimate full field emissions, and then the paired use of GSA and stable isotopic analysis so as to define the non-magmatic-hydrothermal contribution to these emissions. Currently, this appears to be the best approach to constrain the anomalous magma-hydrothermal non-condensable gas release for total heat and mass flow estimations in the Taupo Volcanic Zone.

2) The use of soil gas surveys for blind geothermal exploration is dependent on soil permeability. If there is a magmatic-hydrothermal CO_2 flux of <100 g m^{-2} d^{-1} at the surface due to low permeability, a soil gas survey that does not analyze the source of the φCO_2 using stable isotopic analysis of the $\delta^{13}C_{CO2}$ may not delineate areas releasing magma-hydrothermal CO_2 from depth. It is therefore appropriate to pair a survey of any φCO_2 with analysis of the $\delta^{13}C\varphi_{CO2}$ as adopted by this study.

3) At Rotokawa the total CO_2 emission (633 ± 16 t d^{-1}) was evaluated using a high spatial resolution survey, producing a total mass flux (125 ± 3 Kg s^{-1}) that matches the upflow rate from numerical models (144 Kg s^{-1} *Seward and Kerrick*, 1996; 105 Kg s^{-1} *Bowyer and Holt*, 2010). At White Island the emission rate for diffuse degassing is consistent with previous estimates (~100 td^{-1}; *Werner et al.*, 2004a) and finds a total CO_2 emission (1230 ± 100 t d^{-1}; plume + soil gas) for the island similar to previous estimates (*Rose et al.*, 1986; *Marty and Giggenbach*, 1990; *Wardell et al.*, 2001*; Werner et al.*, 2004a; *Werner et al.*, 2008a).

4) Areas of high flux are constrained by the use of a high resolution survey and confirm that deep seated permeability as major normal faults and/or crater rim structures are paired with surface thermal features. The magnitude of both heat flow and CO_2 flux decrease with distance from each feature. At RK, deep field faults (*Winick et al.*, 2011) appear to have control over the location of thermal activity (in combination with the location of hydrothermal eruption craters) and subsequent gas release at the surface. At WI the greatest concentration of thermal activity is concentrated above the buried crater rim (*Houghton and Nairn*, 1991) and along the margins of the modern day crater which suggests a connection exists with the shallow magmatic-hydrothermal reservoir that channels fluid along crater rim fault-fracture zones.

5) A mechanism for H_2S fixing exists in areas of diffuse soil degassing, as the concentration of H_2S:CO_2 in fumarole gas is more than is measured in diffuse soil gas emissions.

The culmination of several methods into a detailed soil gas surveys approach that is used here for exploratory assessment and the continued monitoring of non-volcanic and volcanic magma-hydrothermal fields is a powerful tool for contributing to the understanding and further research of these unique and volatile areas.

8. Acknowledgements

Thanks to GNS Science and GeoNet for the use of their equipment, Mighty River Power Limited, Powell Geoscience Ltd., University of Canterbury, D.O.C and Tauhara North No.2 Trust for access to the RK thermal area, pilots and crew from SQDRN 3 RNZAF and Peejay IV and V (White Island Tours) for transport to (and from) White Island, The Buttle Family for access to their private volcano. This study contributes to and is funded by the UC-MRP Source 2 Surface research program. Additional funding is from the Ministry of Science and Innovation's Foundation for Research, Science, & Technology through a TechNZ Scholarship and the University of Canterbury's Mason trust.

9. References

Amundson, R., Stern, L., Baisden, T., Wang, Y., 1998. The isotopic composition of soil and soil-respired CO2. Geoderma, 82 (1-3), pp. 83-114. Http://dx.doi.org/10.1016/S0016-7061(97)00098-0

Bergfeld, D., Evans, W.C., Howle, J.F., Farrar, C.D., 2006. Carbon dioxide emissions from vegetation-kill zones around the resurgent dome of Long Valley Caldera, eastern California, USA. J.Volcanol. Geotherm. Res. 152, 140–156. http://dx.doi.org/10.1016/j.jvolgeores.2005.11.003

Bibby, H.M., Glover, R.B., Whiteford, P.C., 1995a. The Heat Output of the Waimangu, Waiotapu-Waikite and Reporoa Geothermal Systems (NZ): Do Chloride Fluxes Provide an Accurate Measure? Proceedings of the 17th NZ Geothermal Workshop. Pp 91-97.

975 Bibby, H.M., Caldwell, T.G., Davey, F.J., and Webb, T.H., 1995b. Geophysical evidence on
976 the structure of the Taupo Volcanic Zone and its hydro-thermal circulation: Journal of
977 Volcanology

978 and Geothermal Research, v. 68, p. 29–58, http://dx.doi.org/10.1016/0377–0273(95)00007-H

979 Boomer, K., Werner, C. and Brantley, S.L., (2000): CO2 emissions related to the
980 Yellowstone volcanic system; 1, Developing a stratified adaptive cluster sampling plan.
981 Journal of Geophysical Research, 105(B5): 10817-10830.
982 Http://dx.doi.org/10.1029/1999JB900330

983 Bowyer, D., and Holt, R., 2010, Case Study: Development of a Numerical Model by a Multi-
984 Disciplinary Approach, Rotokawa Geothermal Field. Proc. World Geothermal Congress 2010
985 Bali, Indonesia, 25-29 April.

986 Brombach, T., Hunziker, J.C., Chiodini, G., Cardellini, C., Marini, L., 2001. Soil diffuse
987 degassing and thermal energy fluxes from the southern Lakki Plain, Nisyros (Greece).
988 Geophys. Res. Lett. 28, 69–72. http://dx.doi.org/10.1029/2000GL008543

989 Cardellini, C., Chiodini, G., Frondini, F., 2003. Application of stochastic simulation to CO_2
990 flux from soil; mapping and quantification of gas release. J. Geophys. Res.108 (B9), 13

991 Castaldi, S., and Tedesco, D., 2005. Methane production and consumption in an active
992 volcanic environment of Southern Italy. Chemosphere, 58(2): 131-139.
993 http://dx.doi.org/10.1016/j.chemosphere.2004.08.023

994 Chiodini, G., Cioni, R., Guidi, M., Raco, B., Marini, L., 1998. Soil CO 2 flux measurements
995 in volcanic and geothermal areas. Appl. Geochem. 13, 543–552. http://dx.doi.org/
996 10.1016/S0883-2927(97)00076-0

997 Chiodini, G., Granieri, D., Avino, R., Caliro, S., Costa, A., Werner, C., 2005. Carbon dioxide
998 diffuse degassing and estimation of heat release from volcanic and hydrothermal systems. J.
999 Geophys. Res. 110 (B8), 17. http://dx.doi.org/10.1029/2004JB003542

1000 Chiodini G, Caliro S, Cardellini C, Avino R, Granieri D, Schmidt A, 2008. Carbon isotopic
1001 composition of soil CO2 efflux, a powerful method to discriminate different sources feeding
1002 soil

1003 CO2 degassing in volcanic-hydrothermal areas. Earth Planet Sci. Lett. 274:372–379.
1004 http://dx.doi.org/10.1016/j.epsl.2008.07.051

1005 Cole, J. W., Thordarson, T., and Burt, R.M., 2000. Magma origin and evolution of White
1006 Island (Whakaari) volcano, Bay of Plenty. New Zealand, J. Petrol., 41(6), 867–895.
1007 http://dx.doi.org/ *10.1093/petrology/41.6.867*

1008 Collar, R.J. and Browne, P.R.L., 1985. Hydrothermal eruptions at the Rotokawa Geothermal
1009 Field, Taupo Volcanic Zone, New Zealand. Proc. 7th NZ Geothermal Workshop. . 1-5.

1010 Dawson, G.B., 1964. The nature and assessment of heat flow from hydrothermal areas. N. Z.
1011 J. Geol. Geophys. 7, 155–171

1012 Deutsch, C.V., Journel, A.G., 1998. GSLIB: Geostatistical Software Library and User's
1013 Guide. Applied Geostatistics Series. Oxford University Press, New York, Oxford.

1014 Donachie, S.P., Christenson, B.W., Kunkel, D.D., Malahoff, A., Alam, M., 2002. Microbial
1015 community in acidic hydrothermal waters of volcanically active White Island, New Zealand.
1016 Extremophiles 6:419–425. Http://dx.doi.org/10.1007/s00792-002-0274-7

1017 Donaldson, I.G. and Grant, M.A., 1978. An estimate of the resource potential of New
1018 Zealand geothermal fields for power generation. Geothermics 7(2-4):243-52.
1019 http://dx.doi.org/10.1016/0375-6505(78)90014-7

1020 Fridriksson, T., Kristjansson, B.R., Armannsson, H., Margretardottir, E., Olafsdottir, S.,
1021 Chiodini, G., 2006. CO 2 emissions and heat flow through soil, fumaroles, and steam-heated
1022 mud pools at the Reykjanes geothermal area, SW Iceland. Appl. Geochem. 21, 1551–1569.
1023 http://dx.doi.org/ 10.1016/j.apgeochem.2006.04.006

1024 Frondini, F., Chiodini, G., Caliro, S., Cardellini, C., Granieri, D., Ventura, G., 2004. Diffuse
1025 CO2 degassing at Vesuvio, Italy. *Bulletin of Volcanology*, 66 (7), pp. 642-
1026 651. http://dx.doi.org/10.1007/s00445-004-0346-x

1027 Giammanco, S., Parello, F., Gambardella, B., Schifano, R., Pizzullo, S., Galante, G., 2007.
1028 Focused and diffuse effluxes of CO 2 from mud volcanoes and mofette south of Mt. Etna
1029 (Italy). J. Volcanol. Geotherm. Res. 165, 46–63.
1030 http://dx.doi.org/10.1016/j.jvolgeores.2007.04.010

1031 Giggenbach, W.F., 1975a. A Simple method for the collection and analysis of volcanic gas
1032 samples. Bulletin Volcanologique, v. 39(1), p. 132-145.
1033 http://dx.doi.org/10.1007/BF02596953

1034 Giggenbach, W.F., 1975b. Variations in the carbon, sulfur and chlorine contents of volcanic
1035 gas discharges from White Island, New Zealand. Bulletin Volcanologique, v 39, p 15-27

1036 Giggenbach, W.F., 1987. Redox processes governing the chemistry of fumarolic gas
1037 discharges from White Island, New Zealand. Appl. Geochem. v. 2(1), p. 143-161

1038 Giggenbach, W.F., 1995. Variations in the chemical and isotopic composition of fluids
1039 discharged from the Taupo Volcanic Zone, New Zealand. Journal of Volcanology and
1040 Geothermal Research, v. 68(1-3), p 89-116

1041 Giggenbach, W.F., and Matsuo, S., 1991. Evaluation of results from Second and Third
1042 IAVCEI field workshops on volcanic gases, Mt. Usu, Japan and White Island, New Zealand.
1043 Appl. Geochem. 6, 125–141. http://dx.doi.org/10.1016/0883-2927(91)90024-J

1044 Giggenbach, W.F., and Sheppard, D.S., 1989. Variation in the temperature and chemistry of
1045 White Island fumarole discharges 1972-85: New Zealand Geological Survey Bulletin, v. 103,
1046 p. 119–126.

1047 Gregg, D.R., 1958. Natural heat flow from the thermal areas of Taupo Sheet District (N 94),
1048 New Zealand Journal of Geology and Geophysics, 1(1):65-75.
1049 http://dx.doi.org/10.1080/00288306.1958.10422795

1050 Hedenquist, J.W., Mroczek, E.K., Giggenbach, W.F., 1988, Geochemistry of the Rotokawa
1051 Geothermal System: Summary of Data, Interpretation and Appraisal for Energy
1052 Development: DSIR Chemistry Division Technical Note 88/6, 64

1053 Hochstein, M.P., and Bromley, C.J., 2005. Measurement of heat flux from steaming ground.
1054 Geothermics 34, 133-160. http://dx.doi.org/10.1016/j.geothermics.2004.04.002

1055 Hochstein, M.P., Mayhew I., and Villarosa, R. A., 1990. Self-Potential Surveys of the Mokai
1056 and Rotokawa High Temperature Fields (NZ). Proceedings of the 12th NZ Geothermal
1057 Workshop.

1058 Houghton, B.F., Nairn, I.A., 1989c. A model for the 1976–82, phreatomagmatic and
1059 Strombolian eruption sequence at White Island volcano, New Zealand. In: Houghton, B.F.,
1060 Nairn, I.A.

1061 .Eds. , The 1976–82 Eruption Sequence at White Island Volcano Whakaari , Bay of Plenty,
1062 New Zealand. N. Z. Geol. Survey. Bull. 103, pp. 127–137, Rotorua

1063 Houghton, B.F., Nairn, I.A., 1991. The 1976-82 Strombolian and phreatomagmatic eruptions
1064 of White Island, New Zealand: Eruption and depositional mechanisms at a 'wet' volcano:
1065 Bulletin of Volcanology, v. 54, p. 25-49.

1066 Inguaggiato, S., A. Mazot, I. S. Diliberto, C. Inguaggiato, P. Madonia, D. Rouwet, and F.
1067 Vita (2012), Total CO_2 output from Vulcano island (Aeolian Islands, Italy), *Geochem.*
1068 *Geophys. Geosyst.*, 13, Q02012, http://dx.doi.org/10.1029/2011GC003920.

1069 Kerrick, D.M., 2001. Present and past non-anthropogenic CO_2 degassing from the solid earth.
1070 *Rev. Geophys.*, 39(4), 565–585. http://dx.doi.org/10.1029/2001RG000105

1071 Krupp, R.E., and Seward, T.M., 1987. The Rotokawa Geothermal System, New Zealand: An
1072 Active Epithermal Gold-Depositing Environment. Economic Geology, 82(5):1109-1129.
1073 http://dx.doi.org/10.2113/gsecongeo.82.5.1109

1074 Lewicki, J. L., Bergfeld, D., Cardellini, C., Chiodini, G., Granieri, D., Varley, N., & Werner,
1075 C., 2005. Comparative soil CO_2 flux measurements and geostatistical estimation methods on
1076 Masaya volcano, Nicaragua. *Bulletin of Volcanology*, *68*(1), 76-90.
1077 http://dx.doi.org/10.1007/s00445-005-0423-9

1078 Lyon, G.L. and Hulston, J.R., 1984. Carbon and Hydrogen isotopic compositions of New
1079 Zealand geothermal gases. Geochemica & Cosmochimica Acta 48, 1161-1171.
1080 http://dx.doi.org/10.1016/0016-7037(84)90052-8

1081 Marty, B., and Giggenbach, W.F., 1990. Major and rare gases at White Island volcano, New
1082 Zealand: origin and flux of volatiles. Geophysical Research Letters Volume 17, Issue 3,
1083 1990, Pages 247-250.

1084 Mazot, A., Rouwet, D., Taran, Y., Inguaggiato, S., and Varley, N., 2011. CO_2 and He
1085 degassing at El Chichón volcano (Chiapas, Mexico): Gas flux, origin, and relationship with

1086 local and regional tectonics, Bull. Volcanol., 73, 423–441. http://dx.doi.org/10.1007/s00445-
1087 010-0443-y

1088 Mörner, N.A., and Etiope, G., 2002. Carbon degassing from the lithosphere. Global Planet.
1089 Change 33, 185–203. http://dx.doi.org/10.1016/S0921-8181(02)00070-X

1090 Rissmann, C.F., 2010. Using Surface Methods to Understand the Ohaaki Field, Taupo
1091 Volcanic Zone, New Zealand. Unpubl. Doctoral Dissertation. Univ. Canterbury,
1092 Christchurch, New Zealand.

1093 Rissmann, C., Nicol, A., Cole, J., Kennedy, B., Fairley, J., Christenson, B., Leybourne, M.,
1094 Milicich, S., Ring, U., Gravley, D., 2011. Fluid flow associated with silicic lava domes and
1095 faults, Ohaaki hydrothermal field, New Zealand. J. Volcanol. Geotherm. Res. 204, 12–26.
1096 http://dx.doi.org/10.1016/j.jvolgeores.2011.05.002

1097 Rissmann, C., Christenson, B., Werner, C., Leybourne, M., Cole, J., Gravley, D., 2012,
1098 Surface heat flow and CO 2 emissions within the Ohaaki hydrothermal field, Taupo Volcanic
1099 Zone, New Zealand, Appl. Geochemistry 27, 223-239.
1100 http://dx.doi.org/10.1016/j.apgeochem.2011.10.006

1101 Rose, W.I., Chuan, R.L., Giggenbach, W.F., Kyle, P.R., and Symonds, R.B., 1986.
1102 Rates of sulfur dioxide and particle emissions from White Island Volcano, New
1103 Zealand, and an estimate of the total flux of major gaseous species, Bull. Volcanol. 48:
1104 181-188. Http://dx.doi.org/10.1007/BF01087672

1105 Rowland, J.V. and Sibson, R.H., 2004. Structural controls on hydrothermal flow in a
1106 segmented rift system, Taupo Volcanic Zone, New Zealand. Geofluids 4:259–283.
1107 http://dx.doi.org/10.1111/j.1468-8123.2004.00091.x

1108 Seward, T.M., and Kerrick, D.M., 1996. Hydrothermal CO_2 emission from the Taupo
1109 Volcanic Zone, New Zealand. Earth Planet. Sci. Lett., 139, 105–113.
1110 http://dx.doi.org/10.1016/0012-821X(96)00011-8

1111 Schmidt, E., Grigull, U., 1979. Properties of Water and Steam in SI-units: 0–800 C, 0–1000
1112 bar. Springer-Verlag, Berlin Heidelberg, R. Oldebourg, München

1113 Sheppard, D.S., Faivre-Perriet, R.X., Orange, C.J., Le Guern, F., 1990. Soil gas surveys: A
1114 cheaper alternative to geophysical surveys: Three examples from the Taupo Volcanic Zone.
1115 Proceedings of the 12th NZ Geothermal Workshop.

1116 Sinclair, A.J., 1974. Selection of thresholds in geochemical data using probability graphs. J.
1117 Geochem. Explor. 3, 129–149.

1118 Thompson, S.K., 1990. Adaptive cluster sampling. J. Am. Stat. Assoc. 85, 1050-1059.
1119 http://www.jstor.org/stable/2289601

1120 Viveiros, F., Cardellini, C., Ferreira, T., Caliro, S., Chiodini, G., & Silva, C., 2010. Soil CO_2
1121 emissions at furnas volcano, São Miguel Island, Azores archipelago: Volcano monitoring
1122 perspectives, geomorphologic studies, and land use planning application. *Journal of*
1123 *Geophysical Research B: Solid Earth*, *115*(12). http://dx.doi.org/10.1029/2010JB007555

1124 Wardell, L.J., Kyle, P.R., Dunbar, N., Christenson, B., 2001. White Island volcano, New
1125 Zealand: carbon dioxide and sulphur dioxide emission rates and melt inclusion studies.
1126 Chem. Geol. 177, 187–200. http://dx.doi.org/10.1016/S0009-2541(00)00391-0

1127 Welles, J.M., Demetriades-Shah, T.H. and McDermitt, D.K., 2001. Considerations for
1128 measuring ground CO_2 effluxes with chambers. Chemical Geology, 177(1-2): 3-13.
1129 http://dx.doi.org/10.1016/S0009-2541(00)00388-0

1130 Werner, C., Brantley, S.L., Boomer, K., 2000. CO_2 emissions related to the Yellowstone
1131 volcanic system. 2. Statistical sampling, total degassing, and transport mechanisms. J.
1132 Geophys. Res. 105, 10,831–10,846.

1133 Werner, C., Cardellini, C., 2006. Comparison of carbon dioxide emissions with fluid upflow,
1134 chemistry, and geologic structures at the Rotorua geothermal system, New Zealand.
1135 Geothermics 35, 221–238. http://dx.doi.org/10.1016/j.geothermics.2006.02.006

1136 Werner, C., Christenson, B., Scott, B., Britten, K., and Kilgour, G., 2004a. Monitoring CO_2
1137 emissions at White Island volcano, New Zealand: Evidence for total decreases in magmatic
1138 mass and heat output, the 11th Symposium on Water-Rock Interaction, Water-Rock
1139 Interaction Working Group of the Int. Assoc. of Geochem. and Cosmochem., Saratoga
1140 Springs, N. Y., 27 June to 2 July.

Werner, C., Hochstein, M.P., Bromley, C.J., Manville, V.R., Tilyard, D., 2004b. CO_2-flux of steaming ground at Karapiti (Wairakei, NZ). Geol. Soc. N. Z. 117A, 115–116

Werner, C., Hurst, T., Scott, B., Sherburn, S., Christenson, B.W., Britten, K., Cole-Baker, J., and Mullan, B., 2008a. Variability of passive gas emissions, seismicity, and deformation during crater lake growth at White Island Volcano, New Zealand, 2002–2006, J. Geophys. Res., 113, B01204, http://dx.doi.org/10.1029/2007JB005094.

Werner, C., Hurwitz, S., Evans, W.C., Lowenstern, J.B., Bergfeld, D., Heasler, H., Jaworowski, C., Hunt, A., 2008b. Volatile emissions and gas geochemistry of Hot Spring Basin,

Yellowstone National Park, USA. Journal of Volcanology and Geothermal Research, 178 (4), pp. 751-762. http://dx.doi.org/10.1016/j.jvolgeores.2008.09.016

Winick, J., Powell, T., Mroczek, E., 2011. The natural-state geochemistry of the Rotokawa reservoir. Proceedings of the 33rd NZ Geothermal Workshop. 16-18 November.

http://www.geonet.org.nz; accessed during 2012

http://www.NIWA.co.nz; accessed during 2011

10. Tables

Table 1: Comparison of sGs and raw total CO_2 emission data by population (as described in results section) at RK. Note that for populations 1-3 of the Raw data, the E_i are within error of the sGs data, but Raw populations 4-5 are an order of magnitude overestimated by the GSA method.

sGs Pop$^{n.}$	1	2	3	4	5
M_i	3.344	16.289	135.693	2319.688	45051.68
σ_1	1.681	7.957	110.310	2456.506	63291.78
CI 95%	0.005	0.012	0.436	18.767	2117.184
f_i (%)	31.4	46.6	17.1	4.6	0.2
S_i (m^2)	449373	668199	245622	65821	3433
E_i (t d^{-1})	1.503	10.885	33.329	152.684	154.662
Raw Pop$^{n.}$	1	2	3	4	5
M_i	3.51	17.749	150.808	2877.491	48200.63
σ_1	1.772	8.282	118.4	3142.717	60240.17
CI 95%	0.158	0.504	9.227	388.346	18314.69
f_i (%)	19.8	42.3	25.8	10.3	1.8
S_i (m^2)	284045	605342	369608	147843	25611
E_i (t d^{-1})	0.997	10.744	55.74	425.417	1234.448

Table 2: Comparison of sGs and GSA total CO_2 emission data by population (as described in results section) at WI. Note that for populations 1-3 of the Raw data, the E_i are within error of the sGs data, but Raw populations 4-5 are an order of magnitude overestimated by the GSA method.

sGs Pop$^{n.}$	**1**	**2**	**3**	**4**	**5**
M_i	0.108	11.159	410.938	5137.417	15008.16
σ_1	.201	8.387	568.366	1364.134	9231.363
CI 95%	.002	.048	2.852	38.575	421.341
f_i (%)	12.7	37.0	48.2	1.5	0.6
S_i (m^2)	40018	117021	152532	4804	1844
E_i (t d^{-1})	.004	1.306	62.681	24.680	27.675
Raw Pop$^{n.}$	**1**	**2**	**3**	**4**	**5**
M_i	.116	11.535	429.216	5157.307	16275.339
σ_1	.206	8.436	581.971	1377.843	10874.412
CI 95%	.002	.038	2.138	27.382	333.593
f_i (%)	9.9	35.0	52.6	1.8	.08
S_i (m^2)	31178	110755	166223	5679	2383
E_i (t d^{-1})	.006	2.188	122.201	50.165	66.436

11. Figures

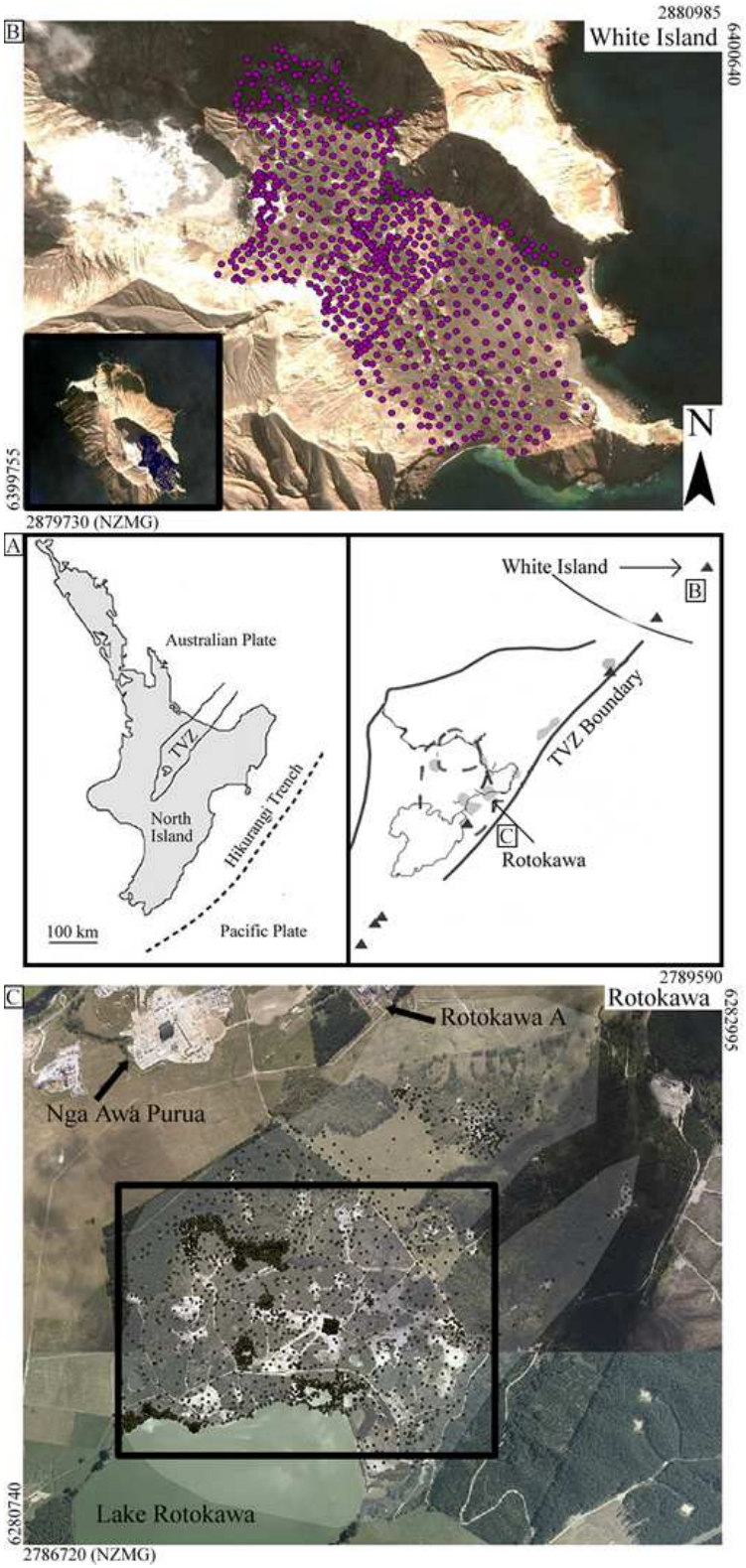

Figure 1: Mapped locations of soil gas measurements at RK (C) and WI (B) with respect to the Taupo Volcanic Zone (A), New Zealand. Black boxes show the area of sGs modeling. Grey shading on RK represents extent of thermal area.

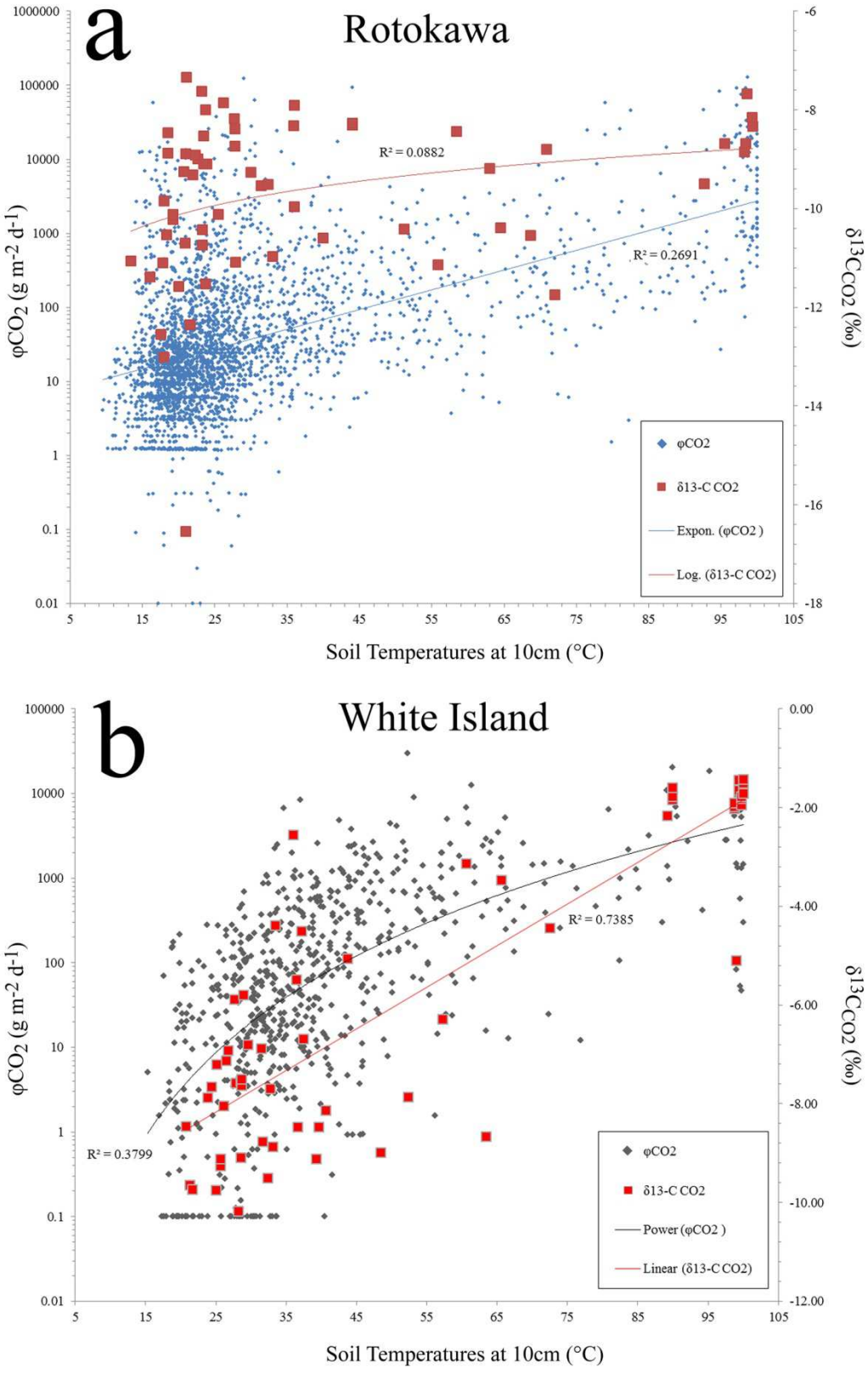

1185

1186 ***Figure 2:*** Plot of soil temperature at 10cm (°C) vs. φCO_2 and $\delta^{13}C_{CO2}$ and coefficient of
1187 determination (r^2) trend lines are shown in respective colors for A) Rotokawa and B) White
1188 Island.

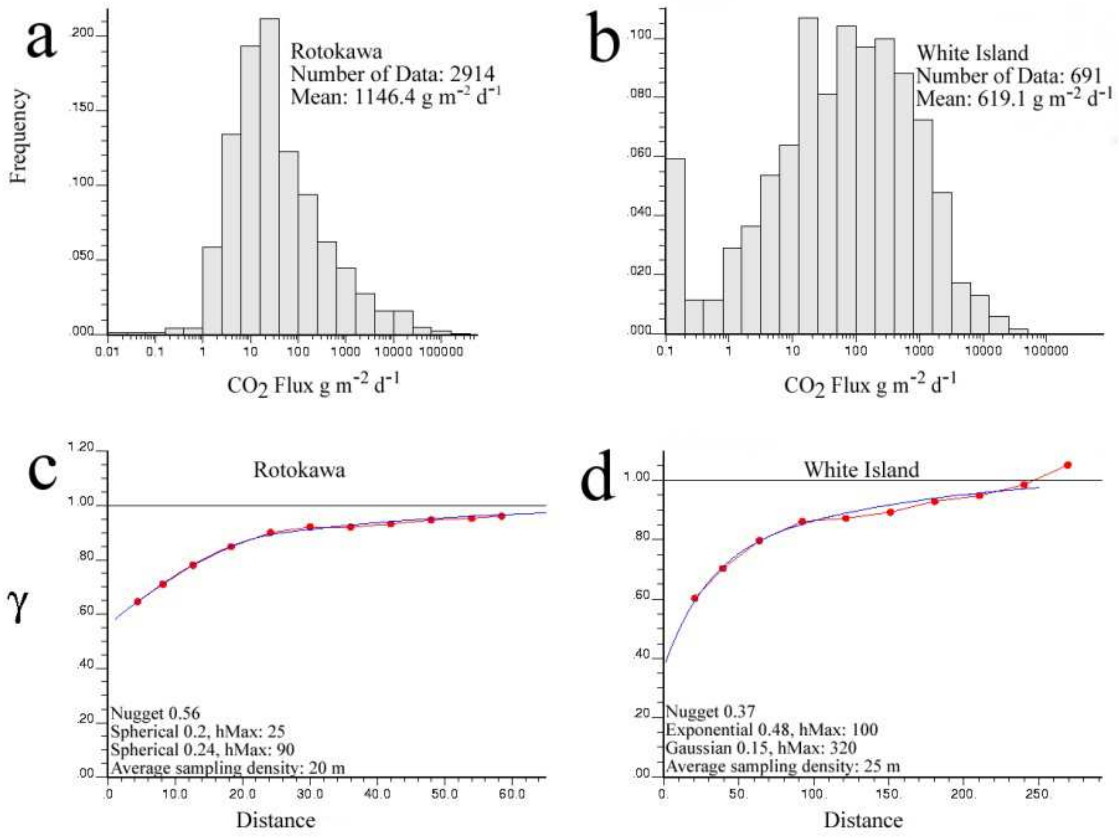

1189

1190 ***Figure 3:*** histograms and variograms for RK (a,c) and WI (b,d). Histograms show statistics
1191 and log-normal distributions. Variogram models used in sGs are in blue and should match the
1192 semi-variograms for the data (red dots and lines)

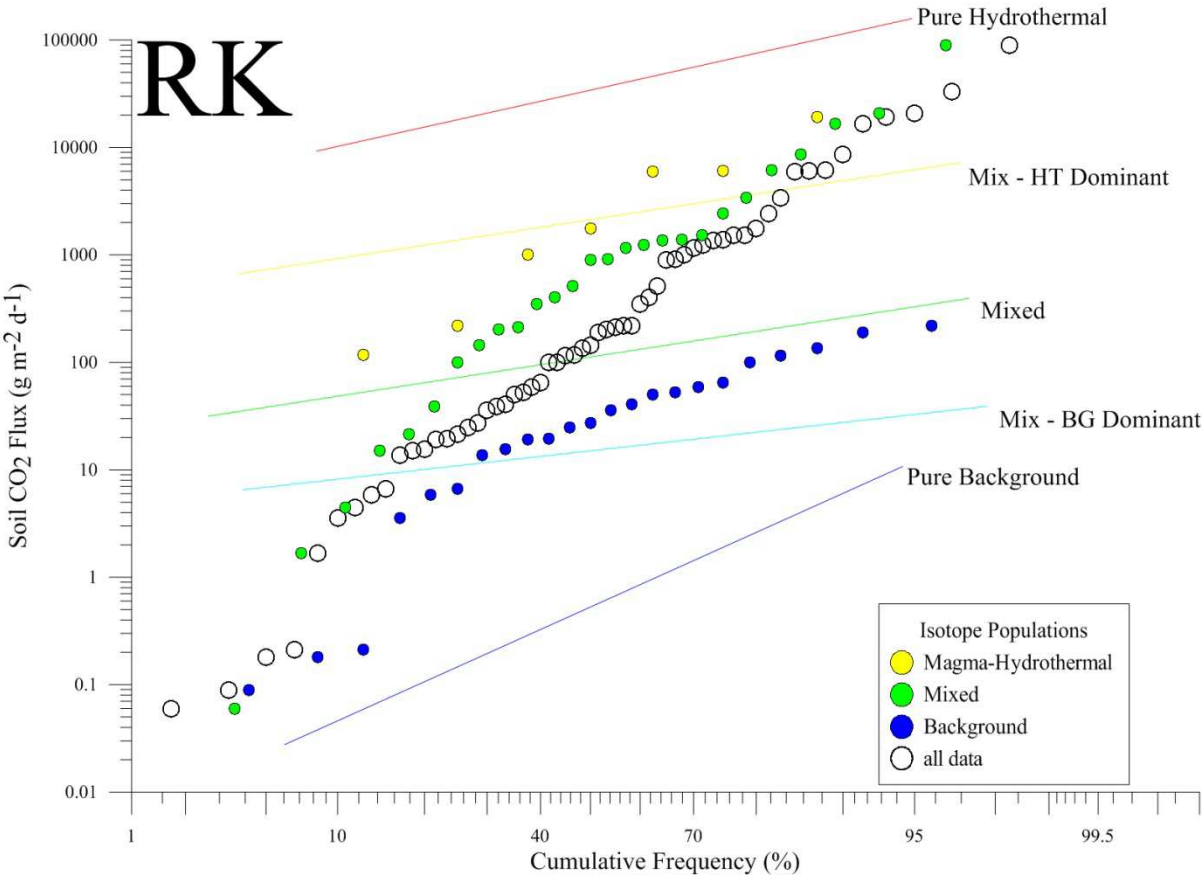

1193

1194 ***Figure 4:*** Cumulative probability plot of the φCO_2 from RK. Empty circles are for all flux
1195 data points where $\delta^{13}C_{CO2}$ was taken (60). Solid lines show the populations partitioned based
1196 on flux values and the GSA method. Filled color circles show the same population
1197 partitioning but by using the $\delta^{13}C_{CO2}$ (per mille, ‰) values.

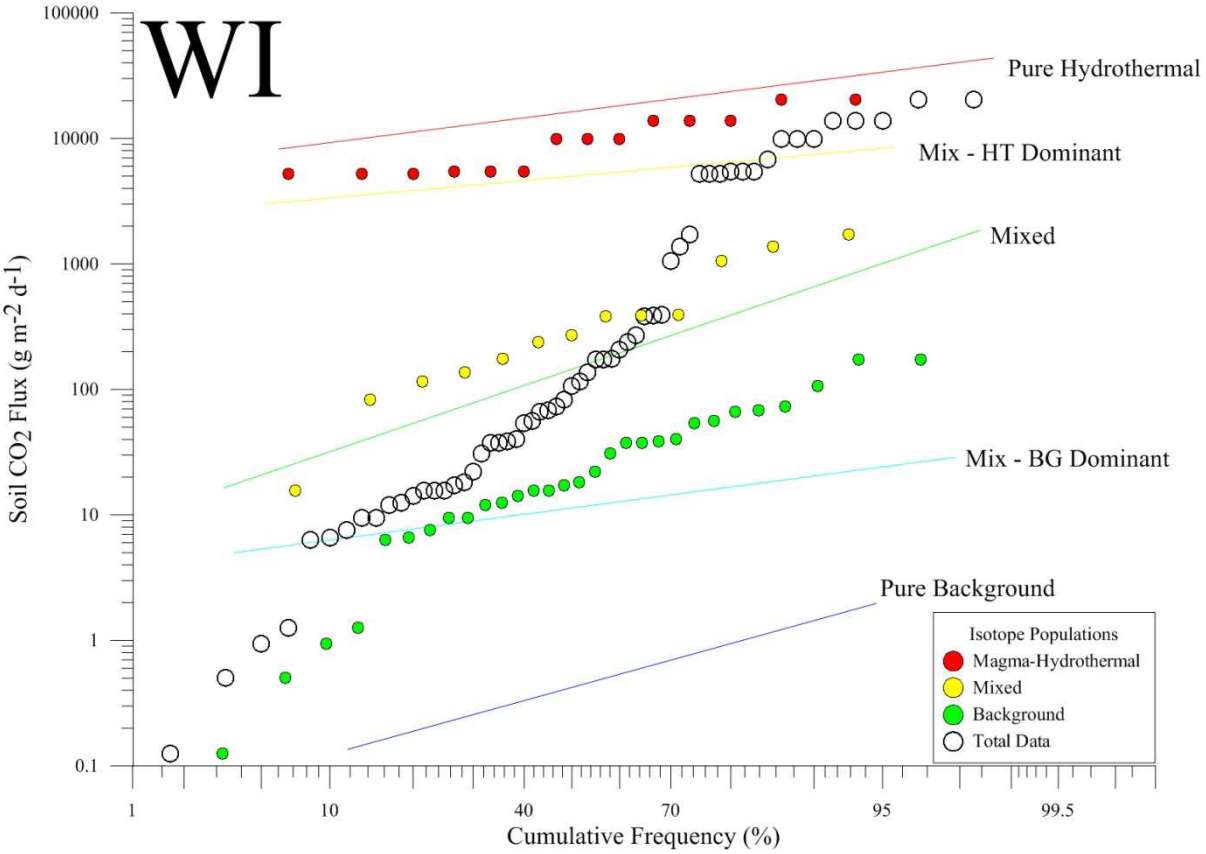

1198

1199 ***Figure 5:*** Cumulative probability plot of the φCO_2 from WI. Empty circles are for all flux
1200 data points where $\delta^{13}C_{CO2}$ was taken (60). Solid lines show the populations partitioned based
1201 on flux values and the GSA method. Filled color circles show the same population
1202 partitioning but by using the $\delta^{13}C_{CO2}$ (per mille, ‰) values.

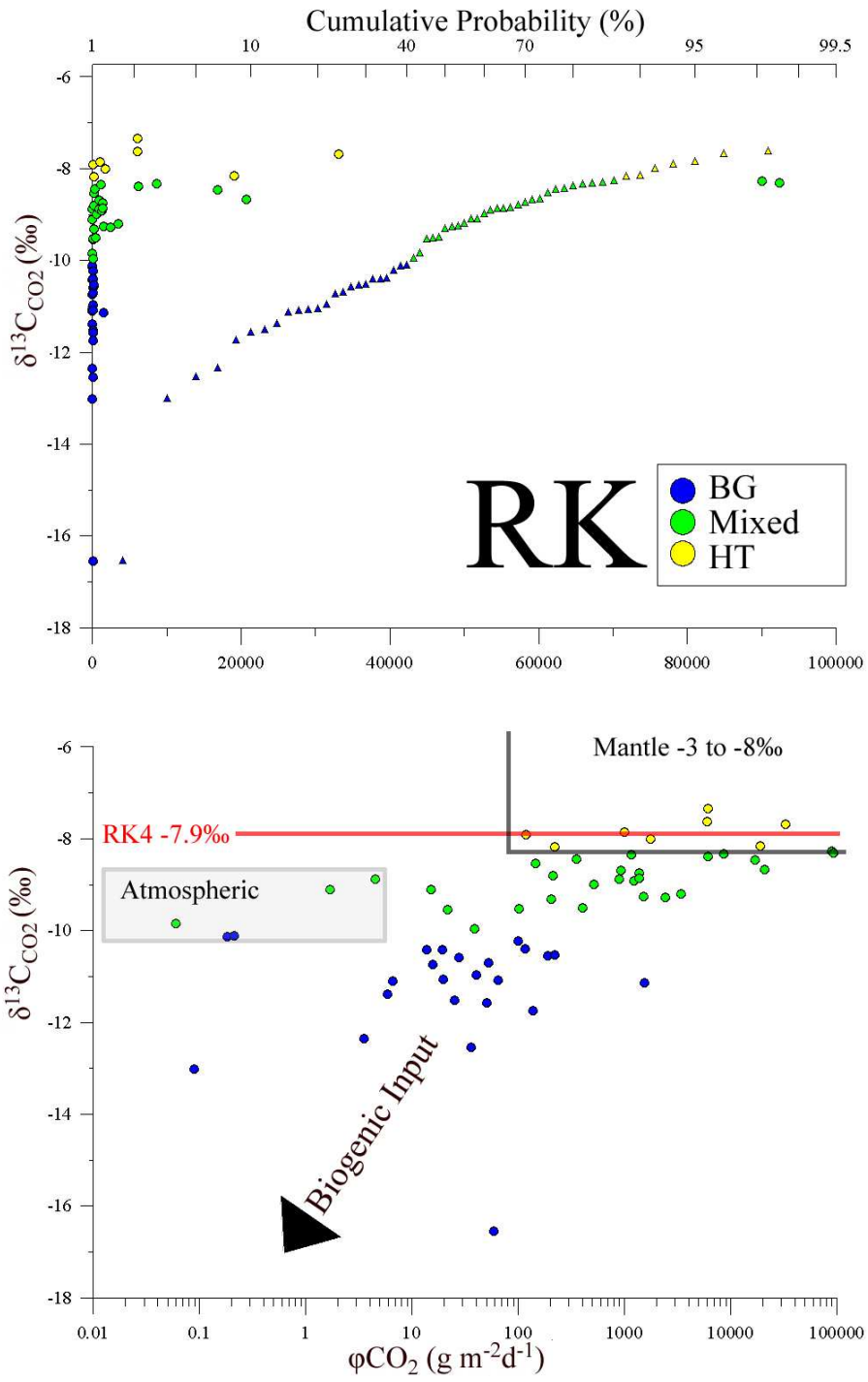

1203

1204 ***Figure 6:*** Diagrams plotting φCO_2 vs. $\delta^{13}C\varphi_{CO2}$, a) All samples are plotted (filled circles) and
1205 show a logarithmic trend when plotted on a linear scale. All samples are plotted (filled
1206 triangles) on a cumulative probability plot and show the inflections that were used to break
1207 the data into populations; b) due to the clustering of data <1000g m^{-2} d^{-1}, a logarithmic scale
1208 is used to show the variation of those fluxes. The fumarole values sampled in *Hedenquist et*
1209 *al.* (1988) for well RK4 is plotted on the diagram to show the reservoir value and best
1210 estimate of the pure hydrothermal source.

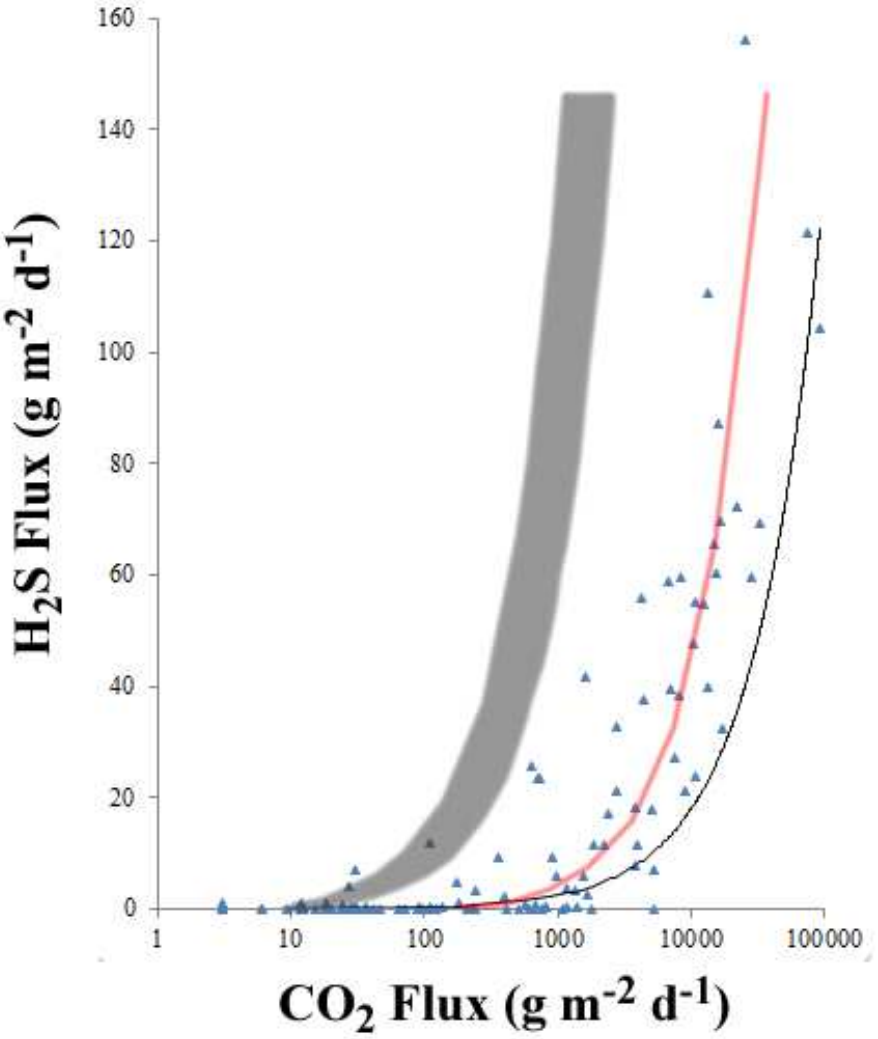

1211

1212 ***Figure 7:*** Distribution of the acid soil gases at RK. The solid grey bar is the estimated fluxes
1213 based on fumarolic gas ratios (max=4.5, min=9.6). The red line is the average diffuse
1214 CO_2:H_2S ratio of 241. The black line is a trend line (power) where r^2=0.65.

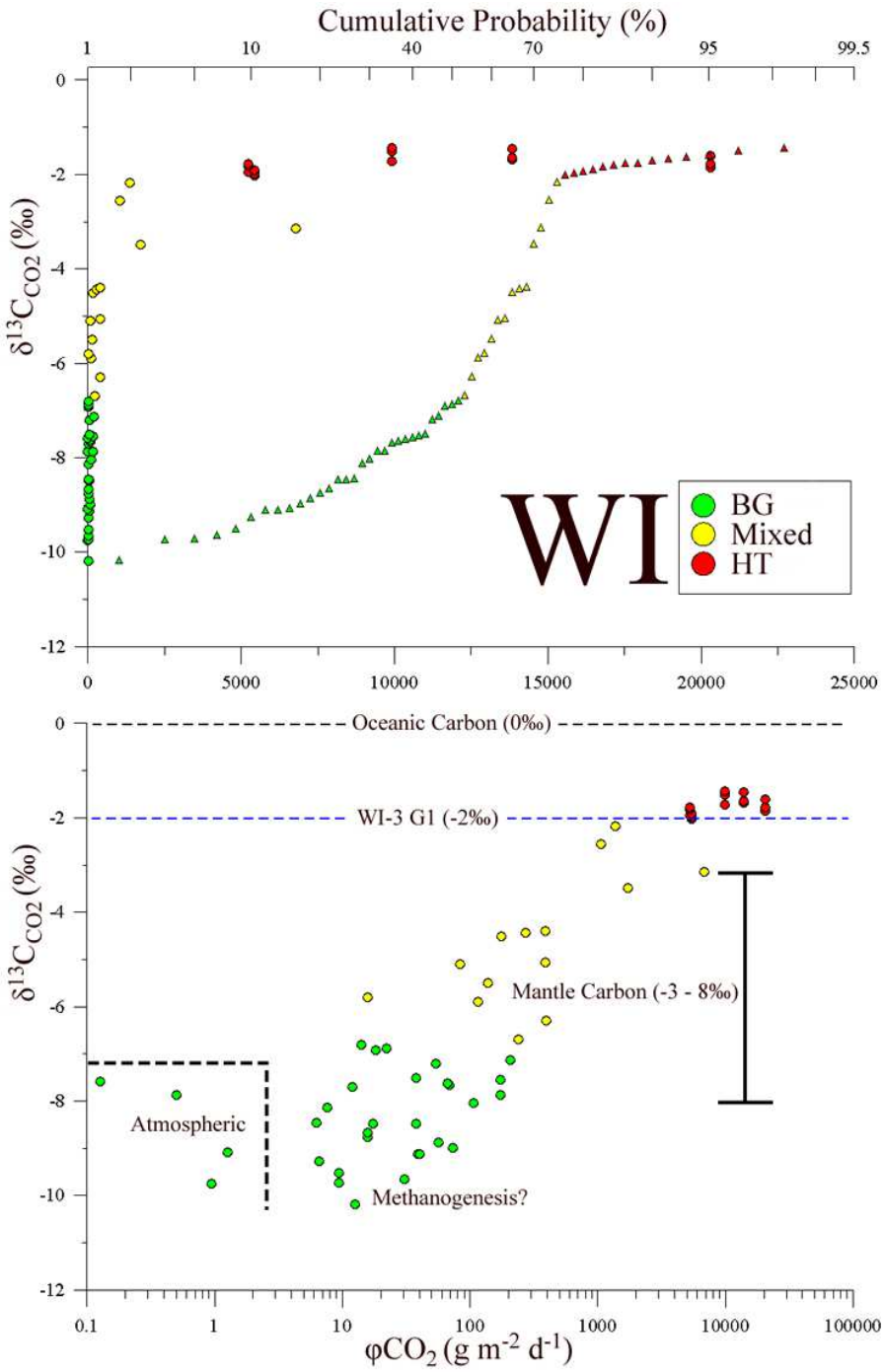

1215

1216 ***Figure 8:*** Diagrams plotting φCO_2 vs. $\delta^{13}C\varphi_{CO2}$, a) All samples are plotted (filled circles) and
1217 show a logarithmic trend when plotted on a linear scale. All samples are plotted (filled
1218 triangles) on a cumulative probability plot and show the inflections that were used to break
1219 the data into populations; b) due to the clustering of data within at low flux (<1000g m^{-2} d^{-1})
1220 range a logarithmic scale is used to show the variation at low flux. The fumarole values
1221 sampled in *Matsuo & Giggenbach* (1991) for WI-3(G1) is plotted on the diagram to show the
1222 reservoir value and best estimate of the pure hydrothermal source.

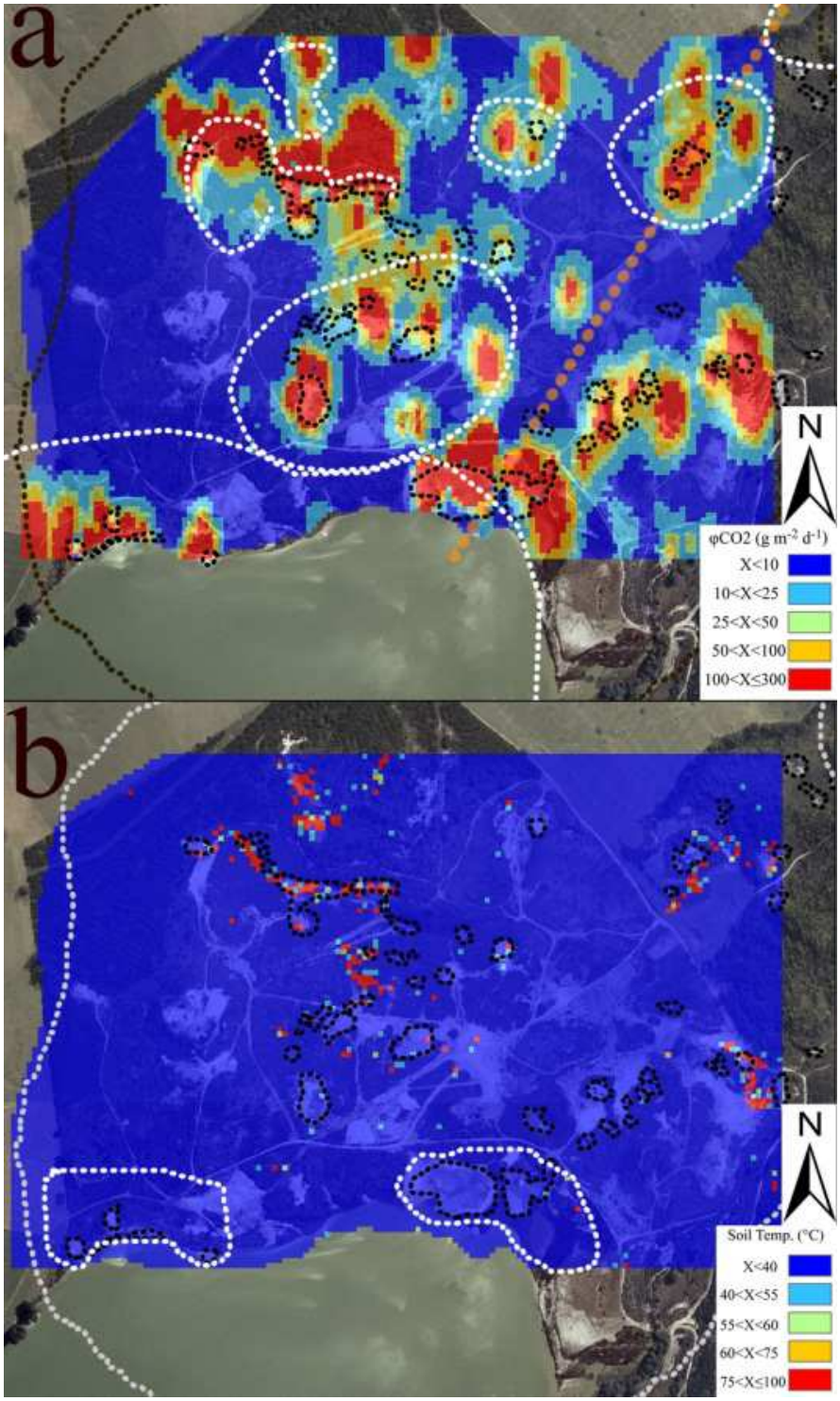

Figure 9, RK: a) φCO_2 mapped within the thermal area's resistivity boundary (*Hedenquist et al.* 1988), the Central Field Fault (CFF) is the orange dotted line, the inferred rims of hydrothermal eruption craters are outlined in white (*Krupp and Seward*, 1987). b) Soil Temperatures at 10cm (°C) are mapped within the thermal areas resistivity boundary. High flux CO_2 anomalies and low temperatures are outlined in white. Surface thermal features are mapped with black dotted lines in each image.

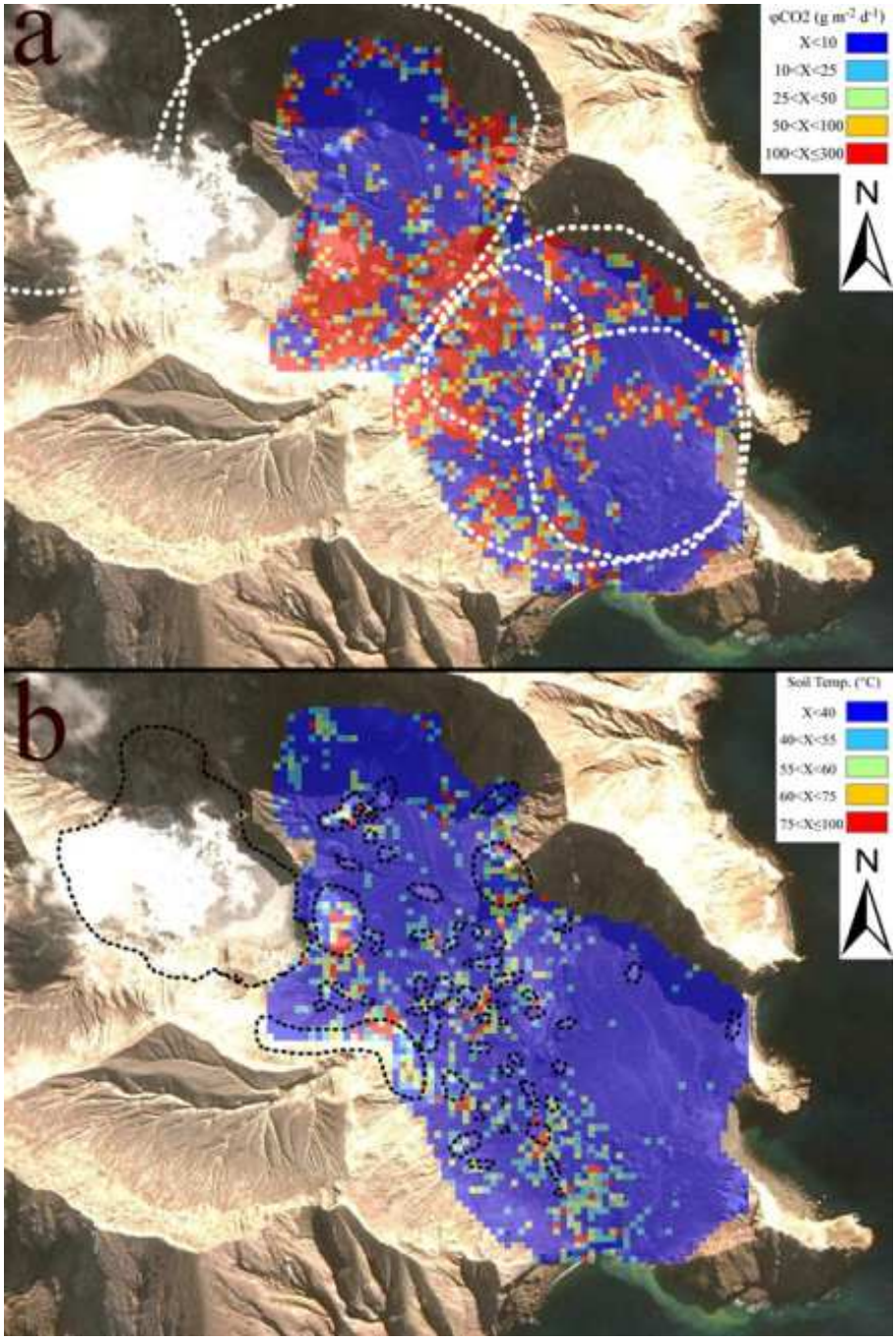

1230

1231 ***Figure 10, WI:*** a) φCO_2 mapped within the accessible crater floor, historic craters are
1232 outlined in white. b) Soil temperatures at 10cm (°C) are mapped within the crater floor;
1233 surface thermal features are mapped with black dotted lines.

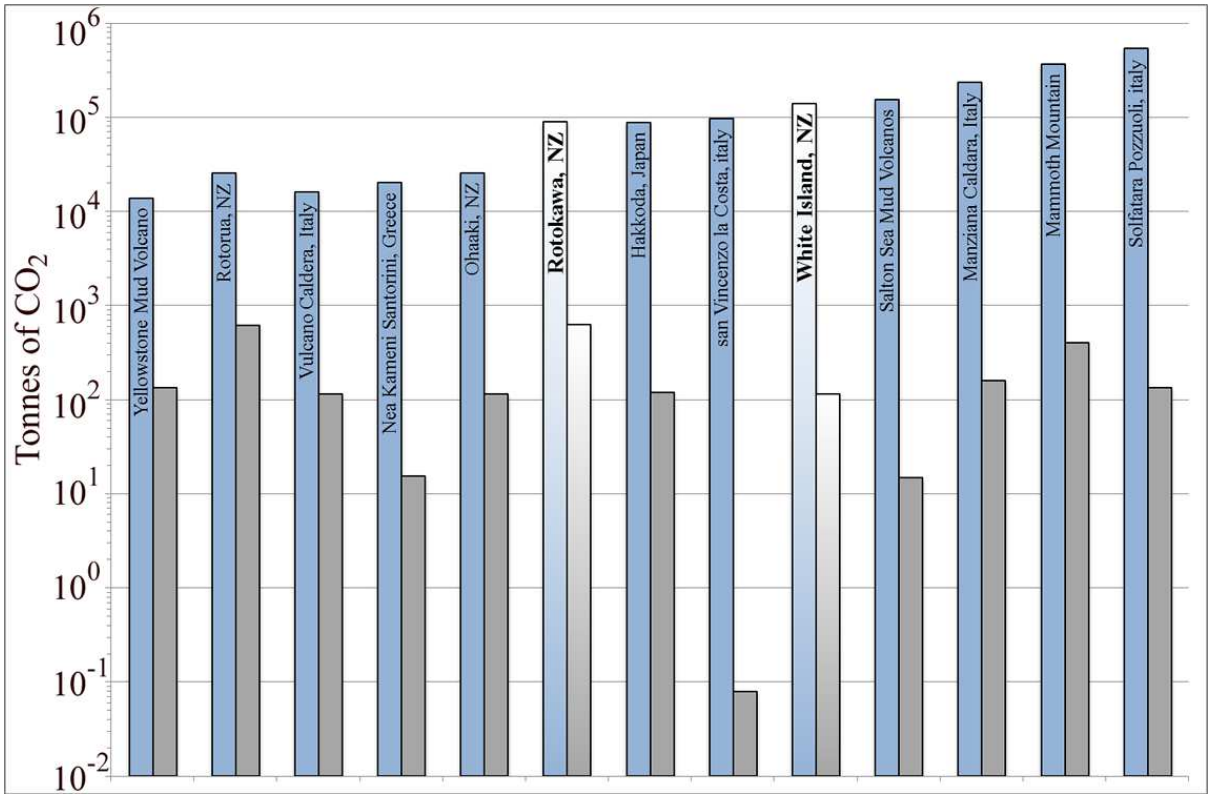

Figure 11: Plot of thermal ground normalized CO2 emissions (blue columns, t yr^{-1} km^{-2}) and total daily CO_2 emission (grey columns, t d^{-1}), this study in graded colours. Modified from *Mörner and Etiope*, 2002*; Rissmann*, 2011.

Future Work

1. Soil gas surveys as a method for quantifying CO_2 emissions

High Resolution Soil gas surveys in New Zealand (>1000 samples km^{-2}; *Rissmann et al.*, 2012; *Bloomberg et al.*, Chapter 1) and even those of moderate resolution (1000>X>100 samples Km^{-2}; *Werner et al.*, 2004; *Werner and Cardellini*, 2006) have increased the values of CO_2 flux from four non-volcanic passive degassing systems in the Taupo Volcanic Zone (TVZ). The use of an accumulation chamber is a fast and robust method (*Welles et al.*, 2001; *Lewicki et al.*, 2005; *Evans et al.*, 2001) for the collection of a direct measurement of the soil CO_2 flux (φCO_2) at fields with permeability from source to surface.

Internationally, φCO_2 surveys have been used in Italy (*Chiodini et al.*, 1998, 2001, 2005, 2008; *Cardellini et al.*, 2003; *Frondini et al.*, 2004; *Giammanco et al.*, 2010; *Carapezza et al.*, 2011; *Inguaggiato et al.*, 2012), USA (*Werner et al.*, 2000*; Bergfeld et al.*, 2001; *Gerlach et al.*, 2001*; Bergfeld et al.*, 2006; *Werner et al.*, 2008; *Evans et al.*, 2009), Greece (*Brombach et al.*, 2001) and Iceland (*Fridriksson et al.*, 2006; *Derienda and Armannsson*, 2010). These surveys are all direct measurements of the passive degassing of volcanic and non-volcanic systems.

In New Zealand, White Island and Rotokawa fields provide ideal locations for the measurement of φCO_2. Data from a recent high resolution study of both fields indicates that these systems contribute significantly to atmospheric CO_2. White Island soil gas emissions are around 10% (40 Kt yr^{-1}) of the total island CO_2 emission (485 Kt yr^{-1}), while Rotokawa emits around 231 Kt yr^{-1}.

The last CO_2 flux estimation of the Taupo Volcanic Zone, New Zealand was by *Seward and Kerrick* (1996) which estimated a total TVZ degassing of 10^{10} mol yr^{-1} (440 Kt yr^{-1}) CO_2. Their method did not directly sample the φCO_2 and instead used measurements of gas contents and mass flows from wells. Recently, other surveys in the TVZ significantly improved on this estimate for the TVZ CO_2 flux (Table 1; *Werner and Cardellini*, 2006; *Rissman et al.*, 2012; *GNS unpublished data*).

While all these surveys were completed in areas with surface thermal areas, it is assumed that CO_2 flux estimations of all geothermal fields in the TVZ have been gross underestimates (as acknowledged in *Seward and Kerrick,* 1996).

2. Estimates for the TVZ from soil gas data

Current estimates for the TVZ's total CO_2 flux have been proven to be an underestimates, initial work to find a more realistic value can start by using the correlation between the non-volcanic systems CO_2 flux and their respective estimated heat flow from chloride flux. In the TVZ this value is CO_2 flux(t d^{-1}) = 2.5 HF (MW_t) in round numbers (Figure 12), where HF is the heat flow from chloride (*Bibby et al.*, 1995) and CO_2 flux is that measured by the previously mentioned four studies (Table 3). Despite CO_2 and heat flux from chloride being collected by different methods and from different surface features, Figure 12 shows a close relationship between these two variables with the the correlation of the four fields having an r^2 value of close to 1. If this relationship were to be applied to all fields in TVZ, a total CO_2 flux of 9400 t d^{-1} or 3,431 Kt yr^{-1} is caluculated from the 4200 MW_t estimated by *Bibby et al.* (1995). This is a 700% increase on the value of *Seward and Kerrick* (1996), however perhaps a more conservative estimate based upon the average % increase from the four fields (320%) where φCO_2 has been measured (Table 3), of 1,412 Kt yr^{-1} is a better minimum estimate for TVZ CO_2 flux.

3. Tables and Figures

Table 3: Comparison of CO_2 flux for non-volcanic systems within the TVZ from *Seward and Kerrick* (1996) and recent soil gas surveys

TVZ System	[1] CO_2 t d^{-1}	Soil CO_2 t d^{-1}	% Increase	[2]Heat Flux (MW_t)
Rotorua	40	620[a]	1558.5399	420
Ohaaki	85	111[b]	129.6895	70
Rotokawa	55	633[c]	1141.5267	300
Tauhara	7	242[d]	3584.8214	110

[1]*Seward and Kerrick* (1996). [2]*Bibby et al.* (1995) [a]*Werner and Cardellini* (2006). [b]*Rissmann et al. (*2012). [c]*Bloomberg et al.* (Chapter 1). [d]*GNS unpublished data.*

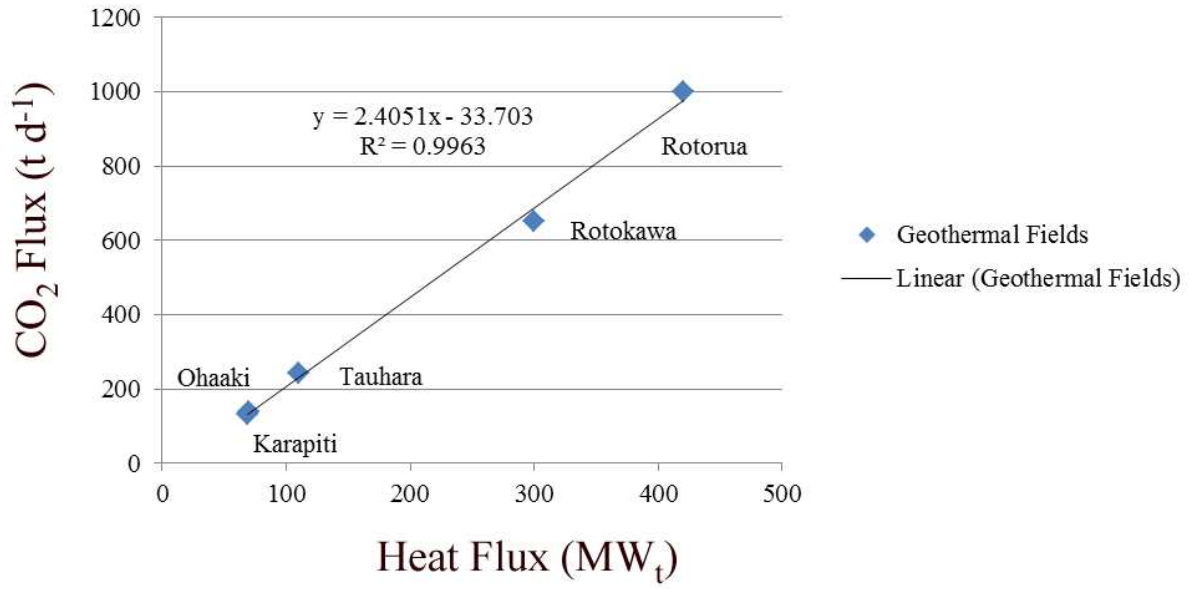

1291

1292 ***Figure 12:*** shows the relationship between directly measured soil gas fluxes from non-
1293 volcanic systems in the TVZ against estimates for heat flow (MW_t) for those fields, data from
1294 Table 3.

1295

Appendix 1

Seawater infiltration at White Island, Bay of Plenty, New Zealand: Using Stable Isotopes of CO_2 and H_2O to evaluate the fluid flow dynamics

[1*]S. Bloomberg., [1]T. Horton., [2]A. Mazot., [1]B. Kennedy., [1]J. Blackstock, [3]C. Rissmann., [1]D. Gravley., and [1]C. Oze.

[1]University of Canterbury, 20 Kirkwood Avenue, Ilam 8041, NZ

[2]Environment Southland, 202 Price Road, Waikiwi 9810, NZ

[3]GNS Science, 114 Karetoto Road, Wairakei 3377, NZ

*E-mail:simonhbloomberg@gmail.com

Contributions:

Mr. Bloomberg conducted the literature review, undertook the field work, geospatial mapping and wrote the manuscript. Dr. Horton undertook the fieldwork, analysed the water samples, and reviewed the manuscript. Dr. Mazot and Dr. Rissmann assisted with the fieldwork and reviewed the manuscript. Dr. Kennedy contributed to the schematic model and reviewed the manuscript. Mr. Blackstock trained Mr. Bloomberg in stable isotope geochemistry and reviewed and contributed to, the manuscript. Dr. Oze and Dr. Gravley enthusiastically reviewed the manuscript. Special thanks also goes to Jelte Keeman and Heather Bickerton (Jan 2011), and Jo Pawson and Mark Letham (Nov 2011) for assisting with fieldwork, and finally to Jim Cole for his keen interest, wealth of knowledge and free perusal of his library over the year!

1. Introduction

Previous investigation of White Island (WI) has described the system as chemically sealed from seawater infiltration (*Giggenbach & Sheppard.,* 1989) by anhydrite precipitation, despite submarine flank vents existing. *Giggenbach et al.* (2003) investigated acid brines in the crater floor of WI and found cause for infiltration of seawater into the shallow hydrothermal system. Recent work on the Plume and crater lake at WI (*Werner et al.,* 2008) found no evidence for seawater infiltration though there was significant evidence of sea level change forcing cyclicity in the CO_2 emission.

1.1 Geological Setting

White Island is an active andesite stratovolcano (Cole et al., 2000) of which <10% of its mass is subaerial due to its location in the Bay of Plenty, 50 km from the nearest landmass. The crater floor is the defining feature of WI and is open to the sea on the SE side where its largely intact crater rim has been breached. The crater floor continues to the W and NW and can be topographically divided in to three large subcraters (Figure 13). Within these subcraters, smaller craters existed which were defined by recent studies (*Houghton & Nairn,* 1991*; Mongillo & Wood,* 1995).

Current volcanic activity in the island is quiescent. Magmatic degassing and conductive heat flow constitutes the main activity by way of a large vapor plume in the far west of the crater floor that emits from a crater lake (*Werner et al.,* 2008). There is a hydrothermal system that extends along the crater floor to the SE from the plume consisting of; steaming mounds, sulphur banks and pools, boiling mud pots, hot springs and a large diffuse CO_2 anomaly (*Bloomberg et al. 2012*).

1.2 Origin of the fluids

Previous studies on White Island have investigated the nature of the shallow hydrothermal subsystem, where magmatic volatiles permeate the soil zone through faults and fractures and advectively and diffusely degas at the surface. Recently, *Giggenbach et al.*

(2003) studied the sources of acid brine spring waters emanating in the crater floor. They found that the high Na of the brines could not be solely attributed to magmatic volatile interaction with rocks during alteration and therefore there must be an interaction with infiltrating seawater within the shallow hydrothermal system. Their stable isotopic analysis of the H_2O found a signature that was reconcilable with *Stewart and Hulston's* (1975) analysis of a seawater contribution to the source of steam condensate, which had previously been discounted (*Giggenbach & Sheppard.,* 1989).

Werner et al. (2008) investigated the nature of the degassing fluids from the crater lake plume found cause for an open system at shallow depths due to external forcing on the degassing caused by sea level fluctuations however the chemistry of the lake and plume indicate no contamination from seawater. Therefore, the plume is shielded from contaminating seawaters by its vapour cloud but within the crater floor the external pressure of magmatic volatiles from the plume is reduced as it flows laterally and magmatic volatiles mix with infiltrating seawater at a ratio of 3:1 (*Giggenbach et al.,* 2003).

Despite evidence for the mixing of seawater with magmatic volatiles (as well as meteoric fluids) their presence was left out of the schematic model of crater and conduit fluid flow dynamics at WI by *Werner et al.* (2008), potentially due to their focus on the crater lake plume, though they did infer input laterally from meteoric waters. It is therefore this studies purpose to investigate the contamination of the hydrothermal system by seawater.

2. Methods

2.1 Soil gas and surface water sample collection

Soil gas samples were taken during the collecting of soil gas flux (φCO_2) measurements suing the West Systems accumulation chamber. A 5 mL syringe was used to pierce a rubber septum on top of the chamber; a gas sample is drawn and emptied into the pierceable butyl rubber septum of a 10mL exetainer vial, pre-conditioned with helium. A fresh needle and syringe is used for each sample. Sampling direct from the chamber was preferred as such surface samples are well-mixed and represent all possible sources of CO_2 (*Chiodini et al.,* 2008).

Surface water samples were taken using a 5 mL syringe, a water sample is drawn and emptied through the pierceable butyl rubber septum of a 10mL exetainer vial.

2.2 Stable Isotopic analysis

The samples were analysed at the University of Canterbury's Stable Isotope laboratory using a Thermo Scientific GasBench II connected to a Delta V Plus gas isotope ratio mass spectrometer under continuous flow conditions was used to measure the deuterium, oxygen and carbon isotopic composition. Stable deuterium, oxygen and carbon isotopic compositions are accurate to <0.10 ‰ based on replicate analysis of NBS-19 and NBS-22 certified reference materials.

3. Results

3.1 Isotopic analysis of soil CO2

Sixty soil gas samples (Figure 12) were analysed for the stable isotopes of CO_2 ($\delta^{13}C_{CO2}$) which were collected concurrently with the φCO_2 and soil temperature. The range of the Stable isotopes and respective soil temperatures and φCO_2 are produced in Table 4. Of those samples 45 were part of the crater floor array, while 15 were triplicate samples of 5 high flux (>1000 g m^{-2} d^{-1}) sites. In this case the averages of the triplicate samples were used and therefore the sample total comes to 50 (Table 4). The triplicate samples were done in order to attain a sense of the uncertainty measureable by the method at high fluxes which ranged from -0.28 to -0.11‰ with a mean of -0.21‰ for $\delta^{13}C_{CO2}$.

Statistical relationships between variables are considered positive with R^2 values of >0.5 for all variables. The highest R^2 is 0.67 when plotting φCO_2 vs. $\delta^{13}C_{CO2}$ and is indicative of a direct connection (Figure 14).

3.2 φCO2 vs. $\delta^{13}C_{CO2}$

White Island (WI) has a complicated source system for CO_2 measured within the crater floor (Figure 14). The heavy end-member, of around -2‰, is attributed to CO_2 release from the hydrothermal reservoir while the Lighter end-member source of around -10‰ (V-SMOW) is thought to be a mix of microbial activity and atmospheric CO_2 into the shallow soil horizon. The sampled data in between describes a mixing population of different proportions of the end member sources. When the isotopic signatures are paired to the φCO_2, the points of high flux are (>1000 g m^{-2} d^{-1}) where there is also a dominantly hydrothermal stable isotopic signature (Figure 14, >-3‰), this is however not a purely proportional relationship and there is an aspect of spatial variability in the data related to permeability of the crater floor.

3.3 Surface water analysis

Fourteen surface water samples were collected and analysed (Figure 13 & Table 5) for stable isotopes of H_2O (δD and $\delta^{18}O_{H2O}$) and dissolved inorganic carbon (DIC) ($\delta^{13}C_{H2O}$). Water data from *Giggenbach et al.* (2003) plot in similar locations to this study (Figure 15). Given that some amount of evaporation is likely to have occurred which would isotopically enrich the fluids, the most likely sources for the acid stream waters are a combination of seawater and magmatic water with minor contributions from meteoric waters. If it was solely magmatic water we would expect to see a strong horizontal shift in the $\delta^{18}O$ data. However, we do see a slight shift to the right and mostly it's an evaporation trend from SMOW.

4. Discussion

4.1 $\delta^{13}C$ analysis of DIC and Flux

Values from stable isotopic analysis of DIC are plotted on Figure 16 and can be related to the $\delta^{13}C\varphi_{CO2}$ in a broad sense. There is some ambiguity in these values as there are multiple spring sources along each flow path that contribute cumulatively to the water sample collected. The range of values indicate a seawater contribution to DIC in the crater floor

springs as already confirmed by the oxygen and hydrogen analysis of *Giggenbach et al.* (2003) and this study (Table 5, Figure 15). Depending on the connectivity depth of the source of the water from the acid springs sampled, the $\delta^{13}C_{H2O}$ will show more or less mixing between meteoric, magmatic and seawater sources. In the western rim of east crater and eastern rim of central crater there is an area of deeper connectivity indicated by the relatively more positive $\delta^{13}C_{H2O}$ compositions. As the water moves East across the crater floor there is an increasing component of meteoric derived fluid to the acid streams as indicated by relatively more negative $\delta^{13}C$.

4.2 Evaluation of fluid flow dynamics

Figure 16 is used to identify any spatial correlations. The area coincident with an old crater rim and the "spring" location on the 2003 (*Giggenbach et al.*) model (which is an area where seawater is mixing with the magmatic volatiles and meteoric water), has the heaviest $\delta^{13}C_{CO2}$ signatures on the island which are all >-3‰. It is hypothesised that seawaters infiltrating the volcanic pile ascend in this area (Figure 17) as it is highly permeable due to its structural history. *Houghton & Nairn* (1991) infer a deep structural fault along the central sub-crater's eastern rim (the area in question) that would provide higher permeability. Interestingly the more seawater-like $\delta^{13}C_{CO2}$ signatures (<2‰) are to the east of the crater rim (Figure 16), perhaps indicating that this structure is acting as a barrier to pure magmatic volatiles in the west side and an open pathway to the mixed seawater and magmatic volatiles from the east. In the west of the central sub-crater, beside the crater lake rim a value of -5.5‰ was sampled which is more indicative of the mixed population or, a magmatic volatile with no seawater contamination, though it is more likely that this is just a more diffuse zone and therefore the sample is more mixed with background sources. *Giggenbach et al.* (2003)'s remarks that the seawater infiltration is 'deep' can be substantiated by the spatial distribution of the "seawater" signature of the diffuse soil CO_2. Only in areas where there is connected permeability to deeper in the system does the $\delta^{13}C_{CO2}$ have a heavy signature. In those places of reduced flux and temperature, where we find a mixed or background signature (e.g. in the east of eastern crater), there is clearly limited permeability to the deeper system.

5. Conclusion

The central sub-crater's eastern rim is a permeable zone of maximum degassing of φCO_2 at WI. Paired to this are enriched $\delta^{13}C$ values which are related to infiltration of seawater into the shallow hydrothermal system. Though *Giggenbach et al.* (2003) have discussed this at length already it has not been fully acknowledged in the literature (*Werner et al.*, 2008) and therefore this relationship of φCO_2 and $\delta^{13}C$ at White Island cements the first presented concept (*Stewart & Hulston*, 1975) and further developed model (*Giggenbach et al.*, 2003) by adding a second variable to the case of seawater entrained in the hydrothermal system at White Island.

6. References

Cole, J. W., Thordarson, T., and Burt, R.M., 2000. Magma origin and evolution of White Island (Whakaari) volcano, Bay of Plenty. New Zeal-and,J. Petrol., 41(6), 867–895. http://dx.doi.org/10.1093/petrology/41.6.867

Chiodini, G., Cioni, R., Guidi, M., Raco, B., Marini, L., 1998. Soil CO 2 flux measurements in volcanic and geothermal areas. Appl. Geochem. 13, 543–552. http://dx.doi.org/10.1016/S0883-2927(97)00076-0

Giggenbach, W., Matsuo, S., 1991. Evaluation of results from Second and Third IAVCEI field workshops on volcanic gases, Mt. Usu, Japan and White Island, New Zealand. Appl. Geochem. 6, 125–141. http://dx.doi.org/10.1016/0883-2927(91)90024-J

Giggenbach, W.F., and Sheppard, D.S., 1989. Variation in the temperature and chemistry of White Island fumarole discharges 1972-85: New Zealand Geological Survey Bulletin, v. 103, p. 119–126.

Houghton, B.F., Nairn, I.A., 1991. The 1976-82 Strombolian and phreatomagmatic eruptions of White Island, New Zealand: Eruption and depositional mechanisms at a 'wet' volcano: Bulletin of Volcanology, v. 54, p. 25-49.

1495 Marty, B., Giggenbach, W.F., 1990. Major and rare gases at White Island volcano, New
1496 Zealand: origin and flux of volatiles. Geophysical Research Letters Volume 17, Issue 3,
1497 1990, Pages 247-250.

1498 Stewart, M.K., and Hulston, J.R., 1975. Stable isotope ratios in volcanic steam from White
1499 Island, New Zealand: Bulletin of Volcanology, v. 39,p. 28–46.
1500 http://dx.doi.org/10.1007/BF02596944

1501

1502 Werner, C., Hurst, T., Scott, B., Sherburn, S., Christenson, B.W., Britten, K., Cole-Baker,
1503 J., and Mullan, B., 2008a. Variability of passive gas emissions, seismicity, and deformation
1504 during crater lake growth at White Island Volcano, New Zealand, 2002–2006, J. Geophys.
1505 Res., 113, B01204, http://dx.doi.org/10.1029/2007JB005094.

1506

7. Tables

Table 4: Descriptive statistics of the variables collected during the soil gas survey at White island.

	ST (°C)	φCO_2 (g $m^{-2}d^{-1}$)	$\delta^{13}C_{CO2}$ (‰)
Min.	20.8	0.125985101	-10.179576
Max.	100	20320.16645	-1.5511435
Mean	43.774	1383.944052	-6.6456796
Conf. Level (95%)	6.98664317	1086.728799	0.72417206
Std. Error	3.47667659	540.7753731	0.36036076
Std. Deviation	24.5838159	3823.859334	2.54813536
C.V.	0.5552	1.6397	0.5493

Table 5: Stable Isotope analysis of springs along the Charter bay outflow. All values are reported in per mille (‰). N/A = Not Analysed

	$\delta^{13}C_{DIC}$	$\delta^{18}O$	$\delta^{2}H$
WI01	-5.35	4.890194	18.40822
WI02	-4.32	5.502718	19.46387
WI03	-3.74	5.725727	20.3074
WI04A	-2.61	5.79873	20.37363
WI04B	-1.6	7.581301	28.50067
WI05	-1.63	5.934735	21.61153
WI06A	-1.58	4.854192	18.58798
WI06B	-2.95	4.482178	18.34299
WI07	-1.14	5.925235	23.51918
WI08A	-3.95	6.763268	25.71713
WI08B	-2.4	5.857732	24.8253
WI09	N/A	5.79523	18.63578
WI10A	-2.41	10.93993	32.46535
WI10B	N/A	10.0289	32.55

8. Figures

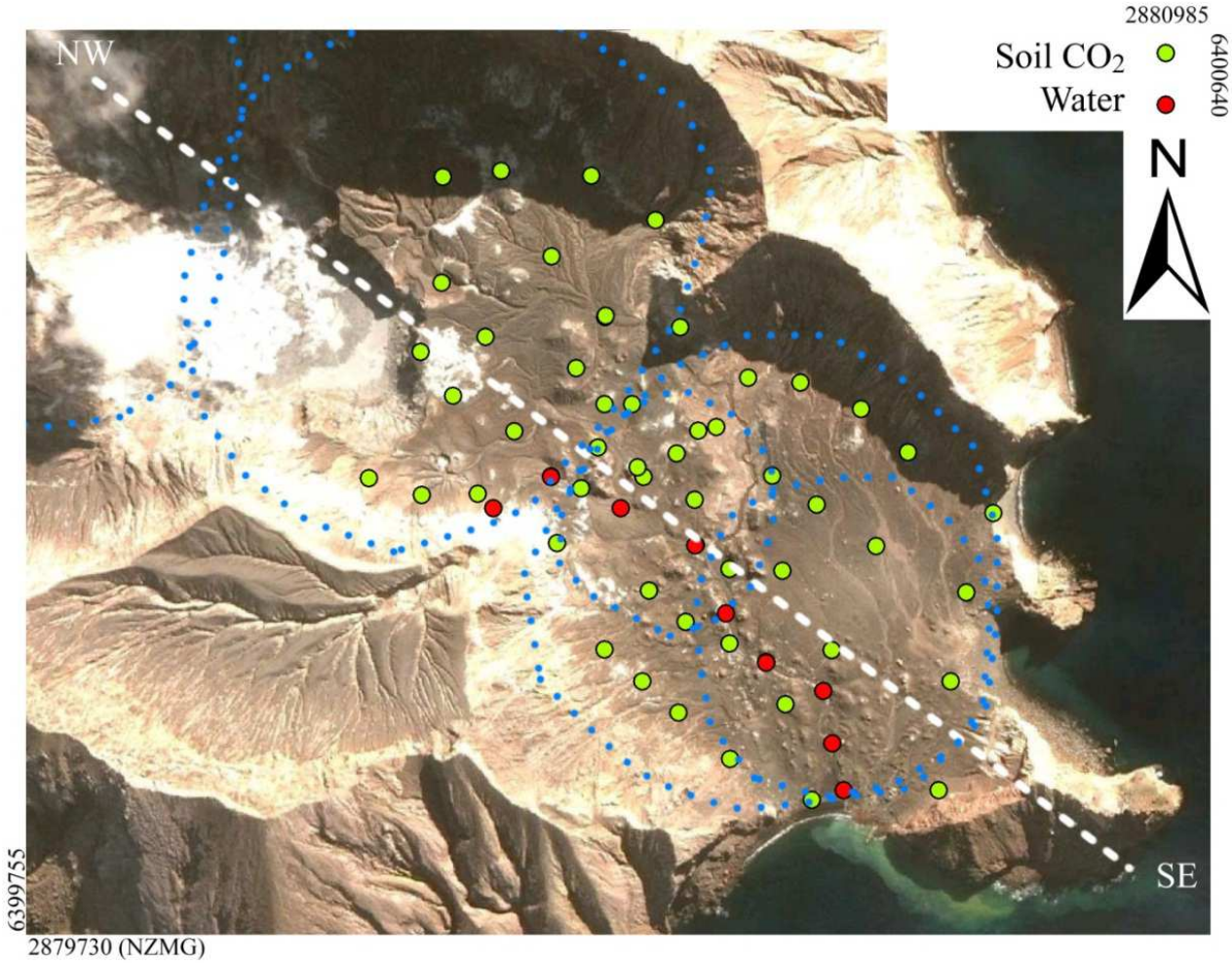

Figure 13: Aerial view of the crater floor at White Island. Soil gas and Water samples are plotted in green and red, respectively. Known crater outlines are detailed by blue dashes, and the x-section for figure 17 is shown in white dash.

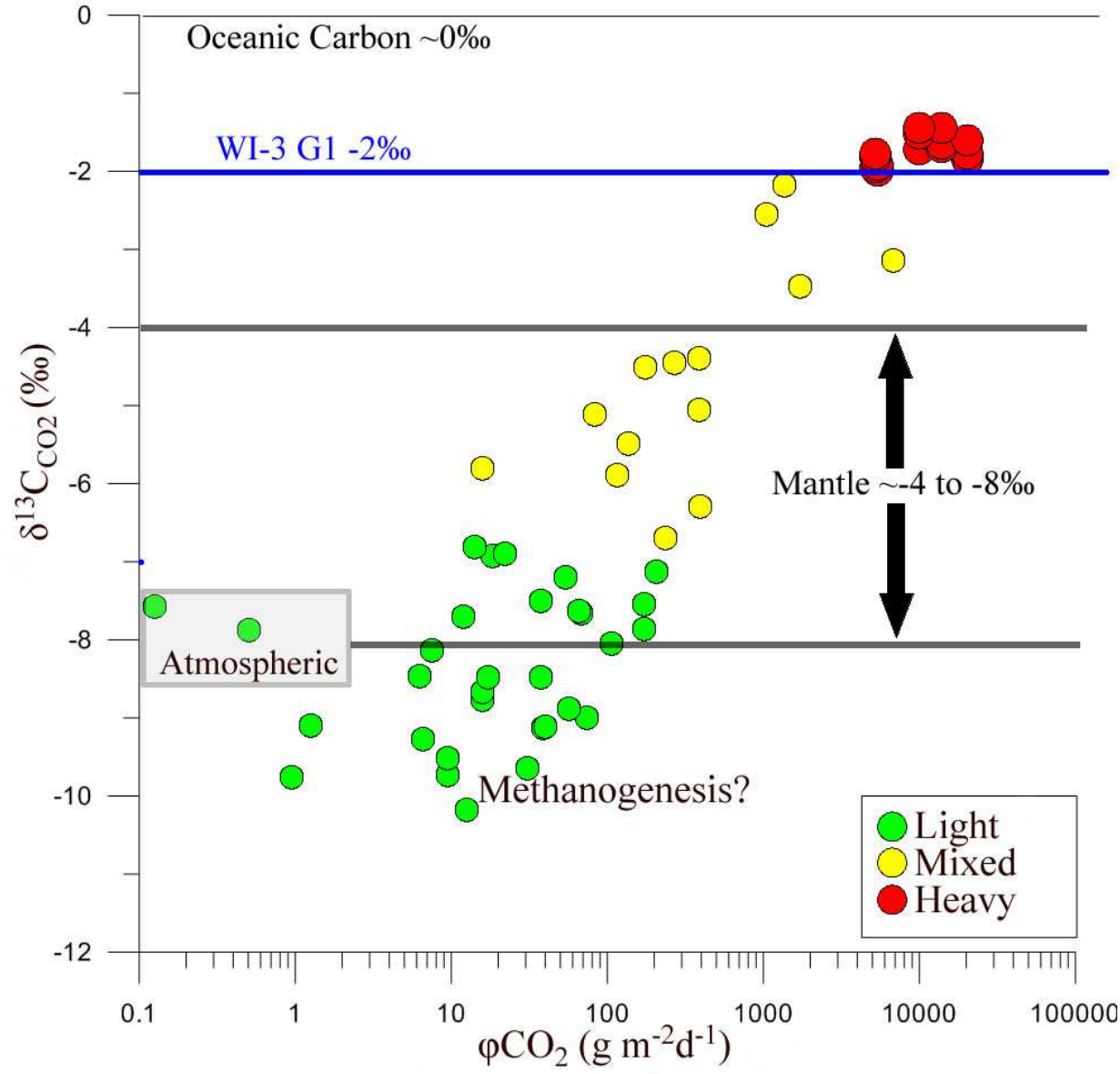

1523

1524 ***Figure 14:*** Plot of φCO_2 vs. $\delta^{13}C_{CO2}$, data is broken into three populations based on the
1525 Graphical Statistical Approach (*Chiodini et al.*, 1998). Each colour represents a population
1526 defined by an inflection on a cumulative probability plot. Sample WI-3 G1 is from *Marty &*
1527 *Giggenbach* (1990)

1528

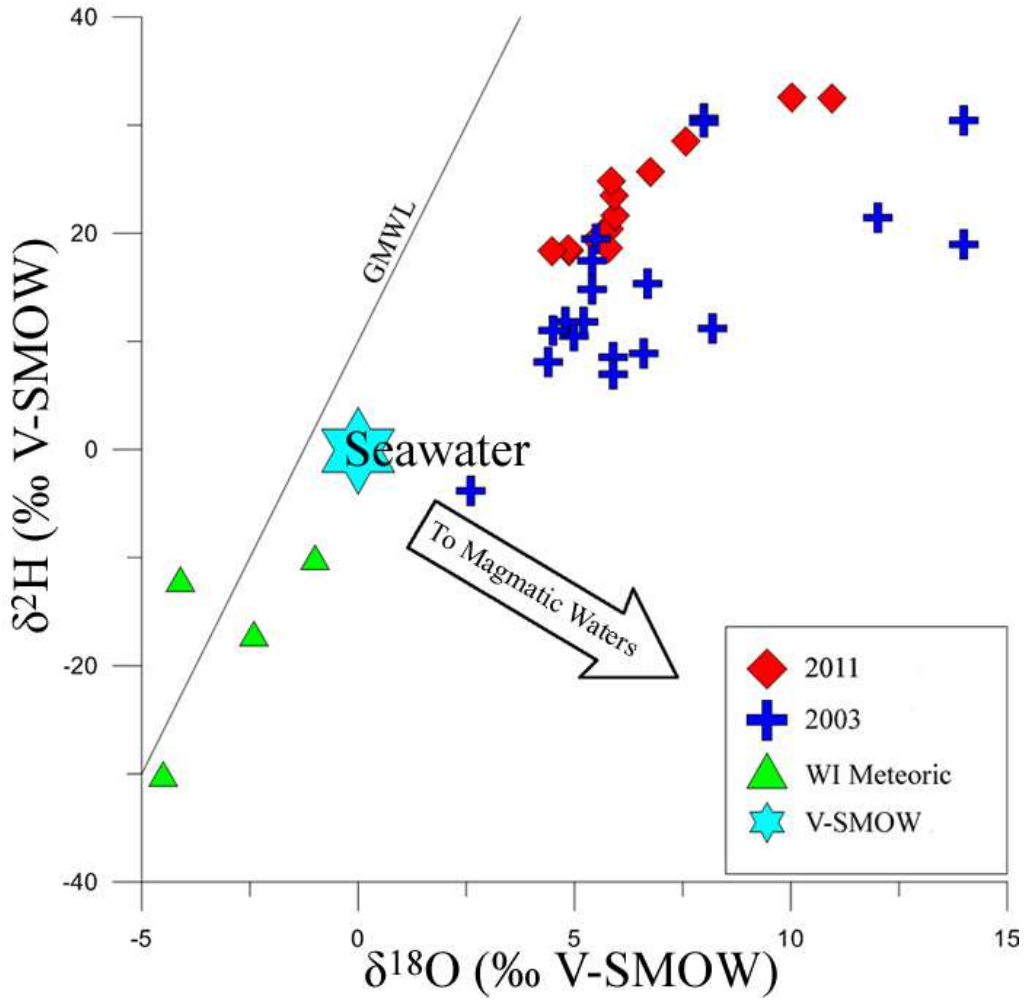

1529

1530 ***Figure 15:*** Hydrogen and Oxygen isotope compositions of waters from White Island. Data
1531 from 2011 and 2003 refer to surface waters sampled by this study and *Giggenbach et al.*
1532 (2003). White Island meteoric samples are collated in *Giggenbach et al.* (2003).

1533

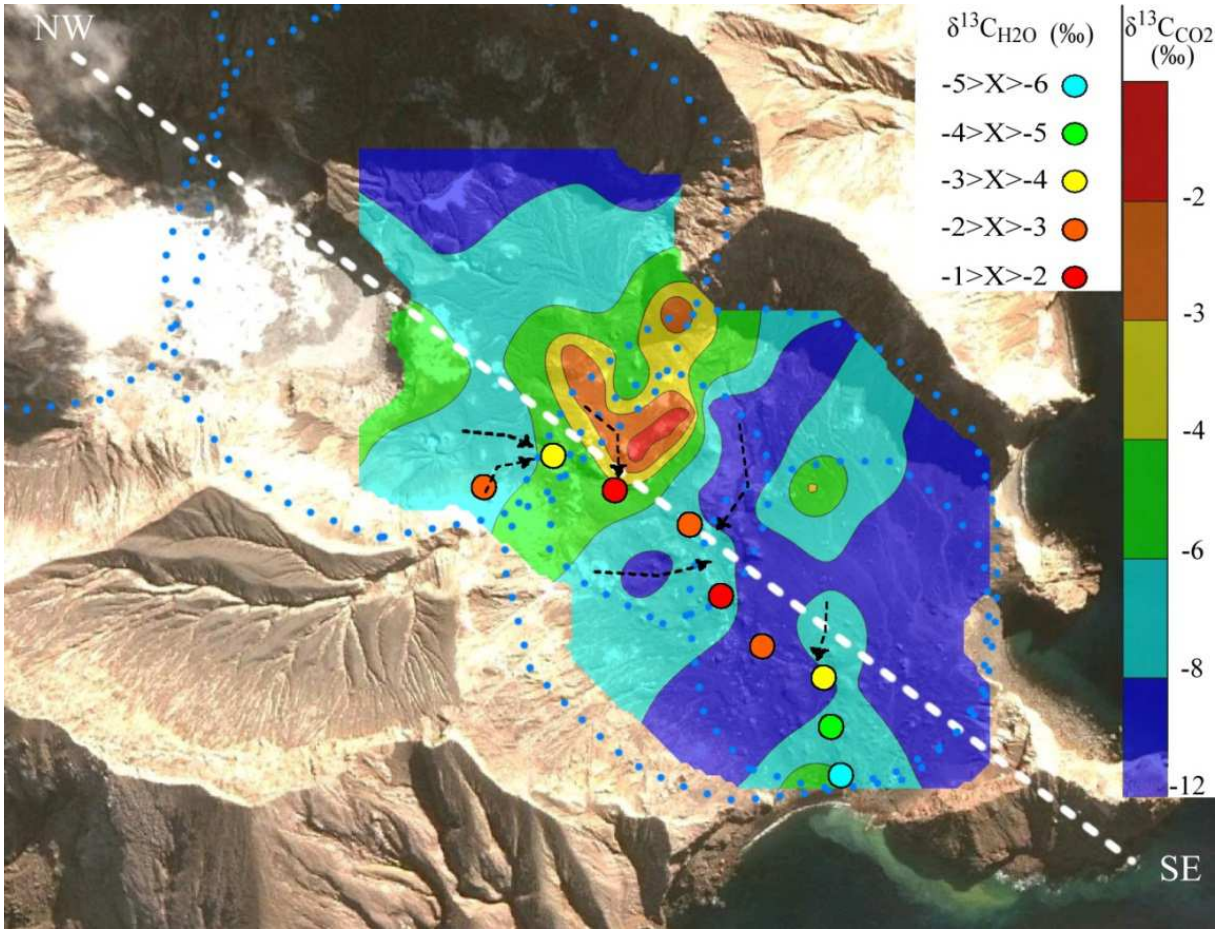

Figure 16: Isoscape of $\delta^{13}C_{CO2}$ within the crater floor. Simple kriging was used in Golden Software's Surfer to interpolate the contours. Surface water samples are plotted as filled circles and black dashed arrows delineate surface water flow lines. Historic craters are outlined in blue dots.

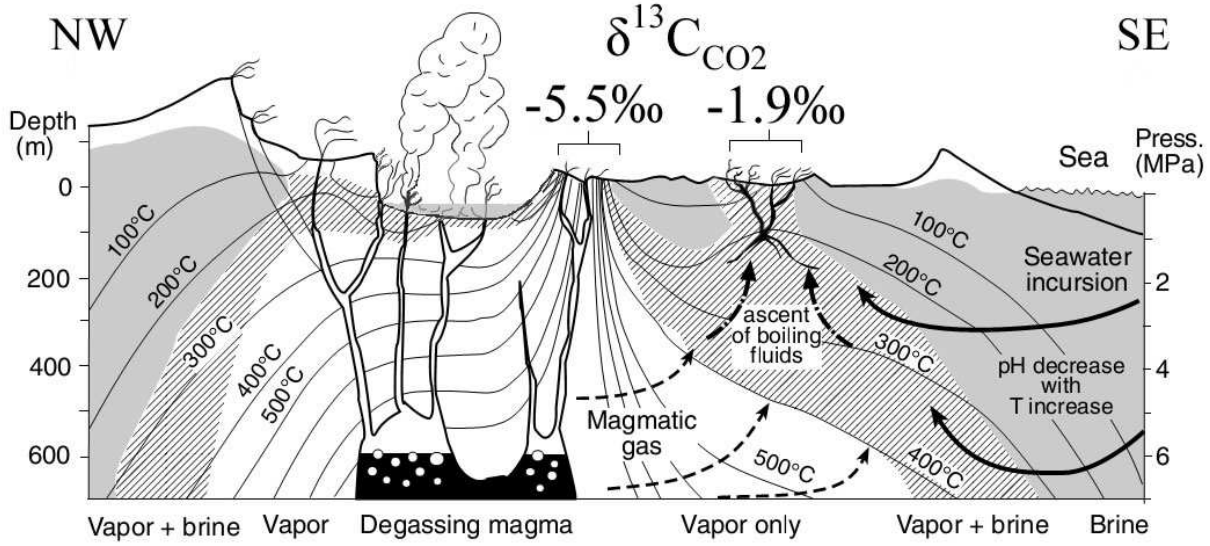

Figure 17: Schematic cross section through the White Island hydrothermal system along the NW-SE line from Figures 13 & 6 (modified after *Giggenbach et al.*, 2003). Solid lines are pure seawater, dashed lines are magmatic volatiles, dashe and dotted lines are a mixture of the two.

Appendix 2

Attached to this thesis is the file “Appendix 2.xlsx”

Within this excel spreadsheet the raw and modified data used in most of the thesis exists. I obviously could not attach the sGs data as it would have made the file huge, however this will be attached in the CD with the bound thesis. Within the file the spreadsheets contained are split by RK for Rotokawa and WI for White island and contain the following:

- RK_Flux: Contains the raw data collected during the soil gas survey campaigns from Cindy Werner in early 2004 through to the data collected in 2011/2012
- RK_Iso: Contains the raw data collected during the soil gas flux and isotope survey during Nov 2011
- RK_H2S: Contains the specific locations and data produced by the H_2S sensor onboard the LICOR.
- RK_SO4: Contains the data used to calculate the sulphur budget for RK
- RK_Results: Contains the sGs data broken into populations by the GSA method, the summation of the total flux into an emission, the extrapolation, and calculation of steam, mass and heat flow values.
- WI_Flux: Contains the raw data collected during the soil gas survey campaign during 2011
- WI_Iso: Contains the raw data collected during the soil gas flux and isotope survey during Nov 2011
- WI_Results: Contains the sGs data broken into populations by the GSA, the summation of the total flux in an emission, the extrapolation, and calculation of steam, mass, and heat flow values.